frontiers | Frontiers in Marine Science

TYPE Original Research
PUBLISHED 21 January 2025
DOI 10.3389/fmars.2024.1511427

OPEN ACCESS

EDITED BY
Meilin Wu,
Chinese Academy of Sciences (CAS), China

REVIEWED BY
Wen-zhuo Zhu,
Zhejiang Ocean University, China
Bo Yang,
Jiangsu Ocean University, China

*CORRESPONDENCE
Chao Wang
chaowang@gdou.edu.cn

RECEIVED 15 October 2024
ACCEPTED 23 December 2024
PUBLISHED 21 January 2025

CITATION
Liu P, Jiang K, Tan Q, Chen F, Jia R and Wang C (2025) Seasonal dynamics of dissolved organic matter in a small tropical estuary-coastal bay continuum: distribution, transformation, flux, and global perspectives. *Front. Mar. Sci.* 11:1511427. doi: 10.3389/fmars.2024.1511427

Seasonal dynamics of dissolved organic matter in a small tropical estuary-coastal bay continuum: distribution, transformation, flux, and global perspectives

Pengfei Liu[1], Kuan Jiang[1], Qi Tan[1], Fajin Chen[1], Renming Jia[2] and Chao Wang[1,2,3,4]*

[1]College of Oceanology and Meteorology, Guangdong Ocean University, Zhanjiang, China, [2]Guangxi Key Laboratory of Beibu Gulf Marine Resources, Environment and Sustainable Development, Fourth Institute of Oceanography, Ministry of Natural Resources, Beihai, China, [3]Key Laboratory of Space Marine Remote Sensing and Application, Ministry of Natural Resources, Beijing, China, [4]Laboratory for Coastal Ocean Variation and Disaster Prediction, College of Oceanology and Meteorology, Guangdong Ocean University, Zhanjiang, China

The export and transformation of riverine dissolved organic matter (DOM) at the river-sea interface are critical to understanding carbon budgets in tropical regions, yet remain underexplored in small watersheds. This study analyzed dissolved organic carbon (DOC), chromophoric (CDOM), and fluorescent DOM (FDOM) over five cruises from summer 2021 to summer 2022 in the Suixi Estuary-Zhanjiang Bay continuum, a eutrophic tropical transition zone in the northwestern South China Sea. Seasonal variations were pronounced for DOM in the continuum and two endmembers. Freshwater DOM, dominated by terrestrial organic materials, was closely tied to soil leaching and erosion, correlating with precipitation patterns. Conversely, seawater DOM, enriched in protein-like FDOM, varied with the West-Guangdong Coastal Current and its associated primary production. Linear decreases in DOM with increasing salinity indicate that conservative mixing largely shapes DOM distributions in the continuum, especially for humic-like FDOM. Non-conservative processes, including flocculation, phytoplankton production, and microbial transformation, variably alter DOM components across seasons. The Suixi River in summer contributed considerably but disproportionately to the annual DOM flux (47-59%), due to intense soil leaching processes that mobilize refractory terrigenous DOM. The deviation observed in the Suixi River's DOC-CDOM relationship from that of global rivers, coupled with a distinctive single-peak pattern between the carbon-specific absorption coefficient and water yield in global rivers, highlights the critical role of watershed nature in influencing river-exported DOM composition. The notably high DOC and CDOM yields for the Suixi River further emphasize the importance of small, tropical rivers in shaping the estuarine and coastal carbon budget.

KEYWORDS

Suixi River, Zhanjiang Bay, dissolved organic carbon, chromophoric dissolved organic matter, fluorescent dissolved organic matter, mixing behavior

1 Introduction

Estuarine and coastal areas play a crucial role in regulating the carbon cycle by controlling the nature and magnitude of terrigenous carbon entering the ocean (Bauer et al., 2013; García-Martín et al., 2021). Dissolved organic matter (DOM), a major reduced carbon pool in these regions, is critical for ecological and biogeochemical functions (Bauer and Bianchi, 2011; Dai et al., 2022). DOM mainly originates from allochthonous sources such as river runoff (Spencer and Raymond, 2024), groundwater discharge (McDonough et al., 2022), atmospheric deposition (Safieddine and Heald, 2017), and anthropogenic activities (Guo et al., 2014), as well as autochthonous production through *in situ* biological activities (Carlson et al., 2024). Given the heterogeneous nature of climate, geography, hydrodynamics, biogeochemical backgrounds, and human pressures, the source, sink, transport, and transformation of DOM in estuarine and coastal areas vary significantly across both temporal and spatial dimensions (Guo et al., 2007, 2014; García-Martín et al., 2021). This variability introduces substantial uncertainties in quantifying the carbon budgets on regional and global scales (Bauer et al., 2013).

River runoff is a major source of allochthonous DOM to the ocean, contributing approximately 260 to 300 Tg C/yr globally (Spencer and Raymond, 2024; Liu et al., 2024). Small rivers, though often overlooked, typically exhibit higher concentrations of dissolved organic carbon (DOC) and contribute significantly to the global flux, especially in tropical regions (Raymond and Spencer, 2015). Tropical rivers have displayed an increasing trend in DOC output over recent decades driven by rising terrestrial organic carbon inputs, even as the global riverine DOC flux generally declines (Li et al., 2019a). Despite their importance, the dynamics of DOC transport by tropical rivers—particularly smaller ones—and their impact on estuaries and coastal bays are not well-studied. This gap is significant considering the vast number of these rivers, their marked seasonality, and their high sensitivity to climate change and human activities (Liu et al., 2024; Spencer and Raymond, 2024).

Riverine DOM, originating from soil and vegetation (i.e., terrigenous DOM), aquatic biological production, and anthropogenic inputs, exhibits considerable diversity in quality, quantity, and biogeochemical reactivities (Li et al., 2019a). Terrigenous DOM, rich in highly unsaturated compounds like lignin phenols and humic acid (Lehmann and Kleber, 2015; Osterholz et al., 2016), predominates in riverine transport to estuaries and coastal bays (Wen et al., 2021). Biological activities (e.g., phytoplankton production, microbial metabolism) could contribute both simple bio-labile molecules (e.g., amino acids, carbohydrate, Rochelle-Newall and Fisher, 2002; Medeiros et al., 2015) and complex bio-refractory molecules (humic substances, Romera-Castillo et al., 2010; Jiao et al., 2024), accounting for ~20% of riverine DOM flux in Chinese rivers (Wen et al., 2021). Anthropogenic inputs could contribute substantial bioavailable DOM to estuarine and coastal systems, especially in regions experiencing increased human activities (Guo et al., 2014; Tzortziou et al., 2015; Wen et al., 2021). Optical analyses results have shown that terrigenous and microbial-derived DOM in abundant in chromophore (i.e., chromophoric DOM, CDOM) and humic-like fluorophores (i.e., fluorescent DOM, FDOM) (Guo et al., 2011, 2014), while the bio-labile DOM components from primary production and anthropogenic inputs are more enriched in protein-like fluorophores (i.e., $FDOM_P$, Guo et al., 2014; Romera-Castillo et al., 2010; Tzortziou et al., 2015). Qualitive optical parameters, such as spectral slope, carbon-normalized absorption coefficient, humification degree, and freshness, provide insights into the source, nature, fate of DOM from land to sea (Helms et al., 2008; Hansen et al., 2016). The optical information has demonstrated a high potential for photochemical and microbial degradations of riverine DOM, thereby influencing its biogeochemical transformation in estuaries and coastal bays (Fichot and Benner, 2014), as well as the actual flux of DOM to the sea (Liu et al., 2024).

Previous studies have shown diverse mixing behaviors of DOM in estuaries and coastal bays across different compounds, spatially and temporally (Guo et al., 2011; Osterholz et al., 2016; Massicotte et al., 2017). Allochthonous CDOM and humic-like FDOM ($FDOM_H$) often exhibit conservative mixing behaviors in various estuaries and coastal bays, as seen in the Mississippi and Atchafalaya River plume regions (Chen and Gardner, 2004), Yangtze River estuary (Guo et al., 2007; 2014), Pearl River estuary (Li et al., 2019b), Jiulong River estuary (Guo et al., 2011), among others (Yamashita et al., 2008; Markager et al., 2011; Zhao et al., 2021). Despite their resistance to microbial utilization (Jiao et al., 2024), these components are susceptible to photodegradation in estuaries and coastal environments (Moran et al., 2000), and may rapidly diminish under favorable conditions of residence time and sunlight exposure (Fichot and Benner, 2014). The priming effect may also accelerate the biodegradation of terrigenous refractory DOM in these regions (Letscher et al., 2011; Bianchi, 2011; Zhuang et al., 2021; Spencer and Raymond, 2024). Additionally, abiotic processes (e.g., sorption-desorption, flocculation) can significantly alter DOM level and compositions in estuaries and coastal environments (McCallister et al., 2006; Asmala et al., 2014). Hence, allochthonous inputs, along with biotic and abiotic transformations, substantially shape the composition, flux, and fate of riverine DOM as it travels from land to sea. These dynamics have been extensively studied in major estuaries like those of Yangtze River estuary and Pearl River estuary (Guo et al., 2014; Li et al., 2019b). However, there remains a significant gap in research across the small river-estuary-coastal bay continuum, especially in tropical regions (Spencer and Raymond, 2024).

In this study, DOC, CDOM and FDOM were measured in the Suixi Estuary-Zhanjiang Bay continuum, a typical tropical estuary and semi-closed bay in the northwestern South China Sea, from summer 2021 to summer 2022. Together with the hydrological and environmental parameters, we aim to (1) investigate seasonal variations of DOM in the freshwater and seawater endmembers; (2) elucidate the distributions and mixing behaviors of DOM using a two-endmember mixing model; and (3) compare the composition, sources, and fluxes of riverine DOM with those from other global rivers.

2 Materials and methods

2.1 Study region

Suixi Estuary-Zhanjiang Bay continuum, situated in the northwest South China Sea (SCS), stands as a tropical estuarine

and coastal bay heavily influenced by human activities. Geographically, the continuum can be divided into two distinct areas: the upper Suixi Estuary and the lower Zhanjiang Bay (Figure 1). The upper estuary experiences a substantial impact from freshwater discharge, predominantly from the Suixi River, with an average annual runoff of 10.4×10^8 m^3. This discharge plays a significant role in shaping the upper continuum's hydrology. In addition, the upper continuum serves as a central hub for oyster breeding activities and is burdened with significant pollution (Lao et al., 2022). Conversely, the lower Zhanjiang Bay is strongly influenced by seawater intrusion from the northwestern South China Sea (SCS), through a narrow channel (~2 km wide), consistently affected by the West-Guangdong Coastal Current (WGCC) persists outside Zhanjiang Bay year-round. During the summer months, this intrusion may intensify pollutant retention within the bay (Lao et al., 2023a). In recent years, there has been a noticeable surge in the discharge of industrial sewage, aquaculture wastewater, and ship navigation wastewater into Zhanjiang Bay, contributing significantly to its pollution load (Zhang et al., 2021). Additionally, the bay's slow water exchange rate promotes nutrient accumulation, exacerbating eutrophication and further degrading water quality (Liang et al., 2024). Consequently, the complex interaction of seasonal variations in river discharge, intrusion of the SCS waters, and human activities results in significant fluctuations in the hydrology, environment, and ecology of Zhanjiang Bay.

2.2 Field observation and sample collection

Five seasonal cruises were conducted in Zhanjiang Bay, located in the northwestern SCS, on the following dates: June 26-30, 2021 (Summer 2021); September 29-October 3, 2021 (Autumn 2021); December 7-10, 2021 (Winter 2021); March 19-21, 2022 (Spring 2022); and June 23-25, 2022 (Summer 2022). Temperature and salinity were measured at twenty-three stations using a calibrated SBE 37 CTD unit (Seabird, USA). Surface water samples (0.5m depth) were collected at all stations using a Niskin bottle, from the upper Suixi River to the offshore SCS. Bottom water samples were obtained at the depth of 1m above the seafloor. Water samples were first collected for dissolved oxygen (DO) analysis. Samples for inorganic nutrient analyses were filtered through MF-Millipore™ filters (0.45 μm) and stored frozen until analysis. Samples for chlorophyll a (Chl-a) and DOM analyses were filtered immediately through pre-combusted (500°C, 5 h) GF/F filters (nominal pore size ~0.7 μm) under a gentle vacuum. Filter membranes for Chl-a samples were stored frozen until analysis. Filtrates were transferred into pre-combusted glass vials with Teflon-lined caps and stored frozen for analyses of DOC, CDOM and FDOM. Analyses of DO and ammonium were completed within 8 hours, and other analyses were conducted within 24 hours of sampling.

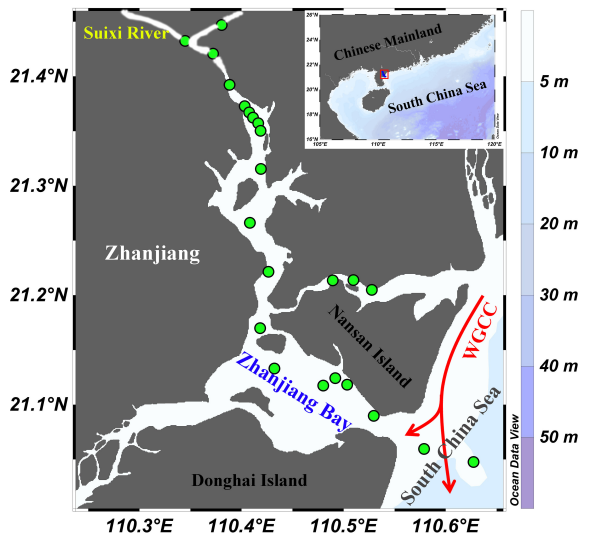

FIGURE 1
Map of sampling stations in the Suixi Estuary-Zhanjiang Bay continuum. WGCC represents the West-Guangdong Coastal Current.

2.3 Measurements of environmental parameters

The DO concentrations were determined using the Winkler titration method (Carpenter, 1965), achieving a precision of 0.07 mg/L. Chl-a was extracted from samples using 90% aqueous acetone, shielded from light, and incubated at 4°C for 24 hours. The Chl-a concentrations were measured with a precision of 0.3 μg/L using a Turner Trilogy fluorometer (Welschmeyer, 1994). The concentrations of nitrate ((NO_3^- - N), nitrite (NO_2^- - N), and soluble reactive phosphate (SRP) were determined using a San++ continuous flow analyzer (Skalar, Netherlands). Ammonium (NH_4^+-N) concentration was measured via spectrophotometry. Dissolved inorganic nitrogen (DIN) was calculated by summing the concentrations of NO_3^- - N, NO_2^- - N, and NH_4^+-N. The nitrogen-to-phosphorus ratio (N/P, mol/mol) was computed as the ratio of DIN to SRP, providing additional insights into the nutrient dynamics. The detection limits for DIN and SRP were 0.05 μmol/L with an analytical precision was better than ± 2%.

2.4 Measurements of DOC

DOC concentrations were determined using a TOC-L_{CPH} analyzer operating in high-temperature catalytic oxidation mode (Shimadzu, Japan). A five-point standard curve was established using potassium hydrogen phthalate standards. DOC concentrations were calculated by first subtracting the running blank, determined as the average peak area of Milli-Q water acidified with HCl, from the average peak area of the samples (injected 2–3 times) and then dividing by the slope of the standard curve. The precision of the DOC analysis was maintained at ±1.0 μmol/L, as validated by DOC Consensus Reference Material (CRM)

provided by D.A. Hansell from the University of Miami (https://hansell-lab.earth.miami.edu/consensus-reference-material/index.html). The coefficient of variation for DOC analysis, based on replicate measurements, was approximately 2%.

2.5 CDOM and FDOM analyses

The absorption spectrum of CDOM was measured at room temperature using a UV-1780 ultraviolet-visible spectrophotometer (Shimadzu, Japan) equipped with a pair of 10-cm quartz cuvettes (L = 0.1 m). Fresh Milli-Q water was served as a blank, with one Milli-Q water sample analyzed after every 5 samples to monitor any potential shifts in the blank. The spectrophotometer scanned from 800 nm to 240 nm at intervals of 0.5 nm. Absorbance values (A_λ) were corrected by subtracting the Milli-Q water blank and were then converted to Napierian absorption coefficients, denoted as a_λ (m^{-1}), using the following formula:

$$a_\lambda = 2.303 \times A_\lambda / L \quad (1)$$

In this study, we report the Napierian absorption coefficients at 350 nm (a_{350}) to quantify CDOM in the Suixi Estuary-Zhanjiang Bay continuum. The choice of a_{350} is due to its frequent use in studies across the land-sea interface (Massicotte et al., 2017). Additionally, the spectral slope between 275–295 nm ($S_{275\text{-}295}$, μm^{-1}) was determined through linear regression of the natural log-transformed absorption spectra (Helms et al., 2008). For broader comparisons, CDOM absorption coefficients at other commonly used wavelengths (e.g., a_{254}, a_{280}, a_{300}, a_{325}, a_{355}, and a_{412}), along with the spectral slope over the range of 350–400 nm ($S_{350\text{-}400}$), are included in Supplementary Table S1. Furthermore, specific ultraviolet absorbance at 254 nm ($SUVA_{254}$, m^2/g C) was calculated by dividing the decadal absorption coefficient (i.e., A_{254}/0.1) by the dissolved organic carbon (DOC) concentration, expressed in mg/L (Weishaar et al., 2003).

Fluorescence excitation-emission matrices (EEMs) of FDOM were measured using an F-7100 fluorophotometer with a 1-cm quartz cuvette at room temperature (Hitachi, Japan). Emission (em) scans were conducted from 280 to 600 nm at 2-nm intervals, paired with excitation (ex) wavelengths ranging from 240 to 450 nm at 5-nm intervals. Both the em and ex slit widths were set to 5 nm. The inner filter effects were corrected following an absorbance-based method (Kothawala et al., 2013). EEMs were then corrected for blank values and normalized using freshly prepared Milli-Q water. Fluorescence intensity was expressed in Raman unit (RU, Lawaetz and Stedmon, 2009).

A total of 203 calibrated EEMs were decomposed using parallel factor analysis (PARAFAC) on MATLAB 2020b with the DOM Fluor toolbox (Stedmon et al., 2003). The model was constrained to nonnegative values, and robustness was confirmed via split-half analysis. Model validation extended to comparing results with published fluorescent components from the Open Fluor database (https://openfluor.lablicate.com/, accessed August 8, 2024; Murphy et al., 2014), using the Tucker Congruence Coefficient (TCC) (Wang et al., 2022). Four qualitative fluorescence parameters derived from EEMs were employed to characterize DOM regarding sources, composition, and reactivity. The humification index (HIX), calculated as the ratio of the integrated emission spectra from 435-480 nm to that from 300-345 nm with excitation at 254 nm, indicating the degree of DOM humification (Zsolnay et al., 1999). The biological index (BIX), computed as the ratio of fluorescence intensity emitted at 380 nm to that emitted at 430 nm upon excitation at 310 nm, providing insights into the presence of fresh biological material in DOM (Huguet et al., 2009). The fluorescence index (FI), calculated as the ratio of emission intensity at 470 nm to that at 520 nm under an excitation of 370 nm, was used to infer DOM source (Cory and McKnight, 2005). Furthermore, the ratio of humic-like fluorescence to protein-like fluorescence (H/P) was calculated, serving as an indicator of the relative abundance of these components within the DOM pool (Hansen et al., 2016).

2.6 River discharge and precipitation data

River discharge data for the Suixi River was source from Wang et al. (2022). Daily precipitation data for the study region was obtained from the China Meteorological Data Service Centre (https://data.cma.cn/). For this study, the cumulative daily precipitation for the 15 days preceding each of the five cruise was calculated.

2.7 Statistical analyses

To assess the significance of differences in environmental and DOM parameters between surface and bottom waters, as well as across different seasons, a two-tailed t-test was applied (α = 0.05), using IBM SPSS Statistics 23. Additionally, Pearson correlation analyses were conducted to explore relationships between DOM variables and salinity, as well as between non-conservative DOM and environmental variables. These analyses were performed using OriginPro 2024b, with significance levels (p-value) determined by a two-tailed test.

3 Results

3.1 Distributions of hydrological and environmental parameters

The Suixi Estuary-Zhanjiang Bay continuum exhibits significant seasonal variations in water temperature, ranging from 20.4°C to 33.4°C throughout the year (Figures 2A–E; Supplementary Figures S1A–E). The highest temperatures were recorded during the summer and autumn, contrasting with the cooler temperatures observed in winter and spring (Table 1). Surface water temperatures were slightly higher than those at the bottom of the continuum (t-test, $p < 0.05$), except for summer 2021 (t-test, $p > 0.05$). Salinity also showed significant seasonal

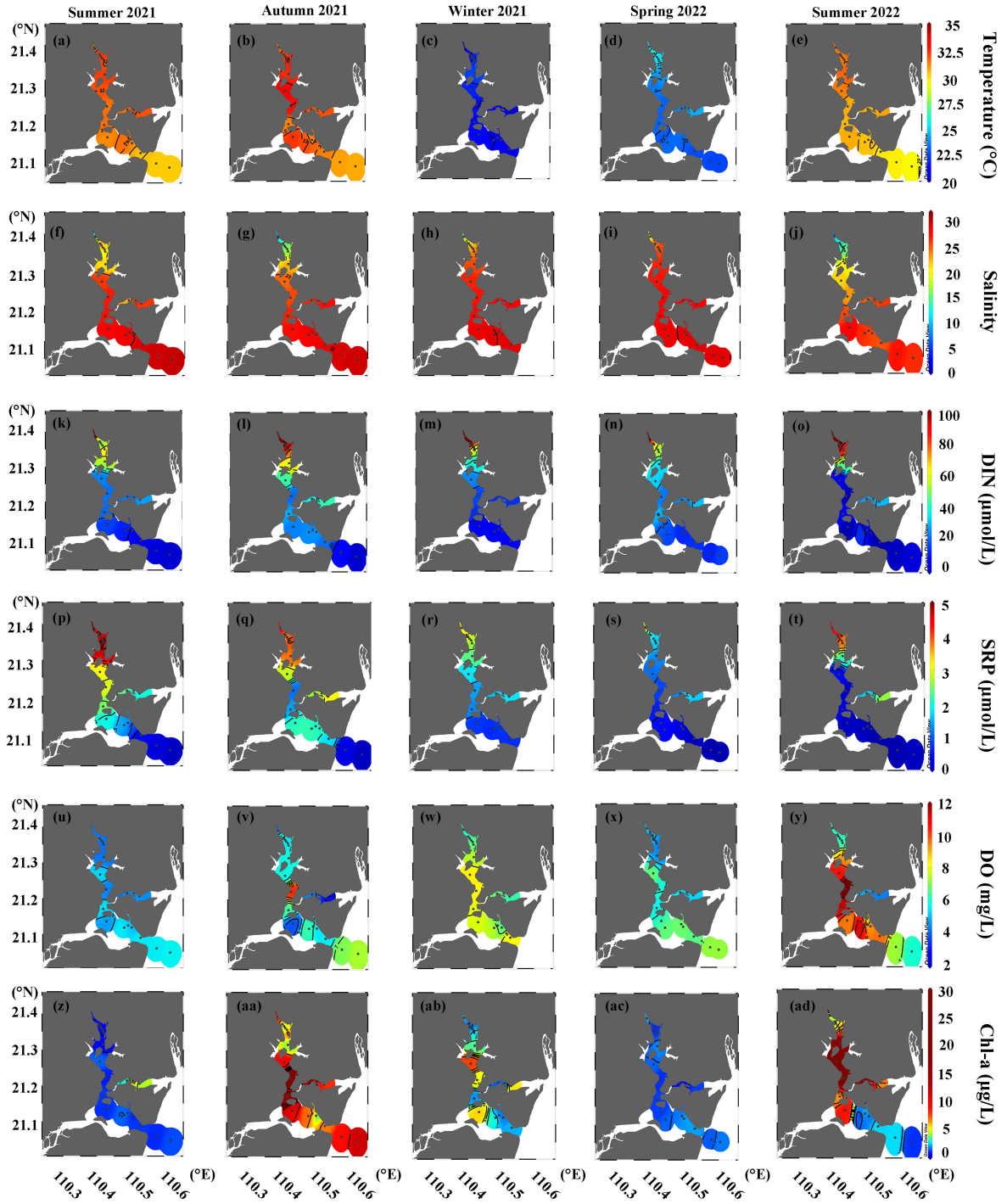

FIGURE 2
Seasonal distributions of **(A–E)** temperature, **(F–J)** salinity, **(K–O)** DIN, **(P–T)** SRP, **(U–Y)** DO, and **(Z–AD)** Chl-a in surface waters of the Suixi Estuary-Zhanjiang Bay continuum.

fluctuations, ranging from 0.4 to 33.1, with lower values typically in summer and autumn and higher in winter and spring. (Table 1; Figures 2F–J; Supplementary Figures S1F–J). A significant difference in salinity between surface and bottom waters is evident across all seasons (*t*-test, $p < 0.05$). This variation was more pronounced in the upper estuary compared to the lower bay (Figures 2F–J; Supplementary Figures S1F–J).

DIN concentrations in the continuum varied widely from 0.3 to 248.5 μmol/L, peaking in autumn 2021 and reaching the lowest in summer 2021 (Table 1; Figures 2K–O; Supplementary Figures S1K–O). SRP concentrations fluctuated between 0.01 and 5.89 μmol/L, with the highest average during summer 2021 and the lowest during spring 2022 (Table 1). Notable differences between surface and bottom DIN levels were observed during winter 2021 and spring 2022 (*t*-test, $p < 0.05$),

10.3389/fmars.2024.1511427

TABLE 1 Ranges and mean values (± SD) of hydrological, environmental, and DOM parameters across fiver seasons in the Suixi Estuary-Zhanjiang Bay continuum.

Parameter	Summer 2021	Autumn 2021	Winter 2021	Spring 2022	Summer 2022
Temperature (°C)	28.4-32.5 31.5 ± 0.9	30.2-33.4 31.7 ± 0.8	20.4-22.5 21.3 ± 0.6	22.4-25.7 24.0 ± 1.17	26.8-31.9 30.7 ± 1.1
Salinity	13.95-31.82 26.12 ± 4.28	4.88-31.21 23.29 ± 7.49	1.80-30.22 24.61 ± 7.30	2.58-30.09 26.50 ± 5.96	0.44-33.13 20.84 ± 8.55
DO (mg/L)	3.67-5.79 4.72 ± 0.59	1.93-10.32 5.16 ± 1.60	5.21-8.49 6.87 ± 0.93	2.47-7.21 5.74 ± 1.06	4.24-12.59 7.42 ± 2.30
Chl-a (μg/L)	0.65-7.75 2.03 ± 2.07	3.66-53.96 12.58 ± 9.36	1.39-22.41 4.58 ± 3.85	0.69-6.84 2.00 ± 1.14	1.39-64.07 13.85 ± 16.69
DIN (μmol/L)	1.6-194.6 42.2 ± 45.6	1.9-160.7 56.06 ± 41.95	5.6-248.5 54.8 ± 64.3	9.9-194.2 45.9 ± 46.2	0.3-195.4 54.1 ± 61.6
SRP (μmol/L)	0.08-5.89 2.90 ± 1.79	0.06-4.53 2.84 ± 1.40	0.66-3.25 1.92 ± 0.94	0.02-4.92 1.28 ± 1.18	0.01-5.00 2.04 ± 1.93
DOC (μmol/L)	77.7-1238.9 327.9 ± 232.0	48.84-536.6 191.63 ± 104.8	55.4-341.1 170.4 ± 62.7	103.4-589.5 190.1 ± 99.5	162.03-504.1 283.7 ± 92.9
a_{350} (m^{-1})	0.43-7.53 1.58 ± 1.57	0.54-5.98 2.29 ± 1.62	0.42-5.24 1.74 ± 1.08	0.59-5.93 1.52 ± 1.21	1.01-7.32 3.28 ± 1.64
C1 (RU)	0.08-1.17 0.33 ± 0.25	0.11-1.34 0.53 ± 0.35	0.10-1.05 0.39 ± 0.23	0.12-1.21 0.31 ± 0.24	0.08-1.12 0.38 ± 0.29
C2 (RU)	0.03-0.51 0.11 ± 0.10	0.03-0.52 0.18 ± 0.14	0.03-0.45 0.15 ± 0.10	0.01-0.50 0.11 ± 0.10	0.03-0.61 0.19 ± 0.16
C3 (RU)	0.02-0.38 0.10 ± 0.08	0.03-0.46 0.17 ± 0.13	0.03-0.43 0.15 ± 0.10	0.03-0.51 0.12 ± 0.11	0.03-0.55 0.18 ± 0.14
C4 (RU)	0.01-0.28 0.12 ± 0.05	0.07-0.30 0.17 ± 0.06	0.07-0.43 0.20 ± 0.09	0.12-0.43 0.17 ± 0.06	0.06-0.47 0.16 ± 0.08
$S_{275\text{-}295}$ (μm^{-1})	12.9-23.9 20.1 ± 2.4	16.3-21.9 19.0 ± 1.9	15.7-22.7 19.8 ± 1.7	16.0-22.1 20.0 ± 1.7	14.2-20.6 17.6 ± 1.4
$SUVA_{254}$ (m^2/g C)	0.24-2.43 0.95 ± 0.44	0.42-6.74 2.16 ± 1.71	1.48-2.52 1.87 ± 0.26	0.98-2.28 1.44 ± 0.26	0.74-2.09 0.951 ± 0.296
HIX	1.17-5.01 2.71 ± 0.97	0.88-5.18 3.12 ± 1.33	1.17-3.56 2.47 ± 0.52	1.39-4.37 2.34 ± 0.75	1.69-6.22 3.45 ± 1.46
BIX	0.79-1.16 1.07 ± 0.08	0.90-1.43 1.05 ± 0.12	0.9.-1.18 1.07 ± 0.06	0.93-1.83 1.16 ± 0.18	0.85-1.42 1.01 ± 0.11
FI	2.46-2.63 2.57 ± 0.04	2.52-2.66 2.58 ± 0.04	2.49-2.68 2.58 ± 0.04	2.50-2.69 2.58 ± 0.04	2.41-2.65 2.53 ± 0.06

whereas SRP concentrations showed no significant variation between depths across any season ($p > 0.05$). Both DIN and SRP concentrations generally peaked near the Suixi River in the upper estuary and decrease towards the seaward direction across all seasons (Figures 2P–T; Supplementary Figures S1P–T).

DO concentrations exhibited seasonal variations ranging from 1.93 mg/L to 12.59 mg/L (Table 1), with peaks in the center of Zhanjiang Bay during autumn 2021 and summer 2022 (Figures 2U–Y; Supplementary Figures S1U-Y). In these seasons, surface water DO concentrations were significantly higher than those in bottom water (*t*-test, $p = 0.008$ and $p = 0.01$, respectively), while no significant differences were noted in other seasons ($p > 0.05$). Chl-a concentrations range from 0.65 μg/L to 64.07 μg/L, peaking during autumn 2021 and summer 2022, with lower concentrations noted during summer 2021 and spring 2022 (Table 1). Significant disparities in Chl-a concentrations between surface and bottom waters were noted in summer 2021 (*t*-test, $p< 0.05$). Corresponding to the observed high DO concentrations, elevated Chl-a levels (> 20 μg/L) were observed in the central continuum during both autumn 2021 and summer 2022 in both surface and bottom waters (Figures 2Z–AD; Supplementary Figures S1Z-AD).

3.2 PARAFAC results

PARAFAC analysis identified four major fluorescent components (Supplementary Figure S2), including three humic-like components (C1, C2, C3) and one protein-like component (C4). C1 exhibited excitation/emission maxima at 270/460 nm, aligning with the typical humic-like peak A (Coble, 2007). C2 displayed two excitation maxima

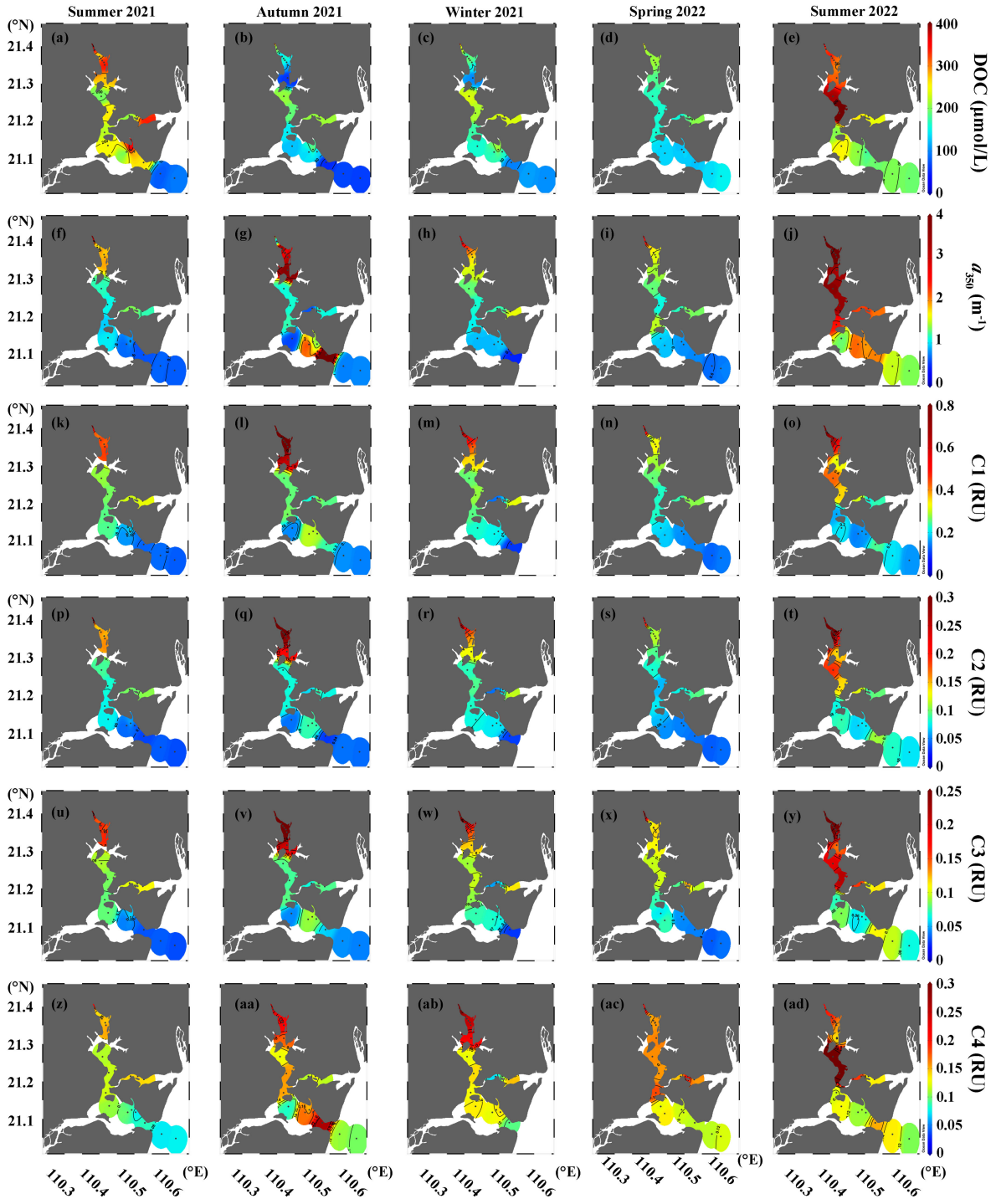

FIGURE 3
Seasonal distributions of **(A–E)** DOC, **(F–J)** a_{350}, and **(K–AD)** intensities of four FDOM components in surface waters of the Suixi Estuary-Zhanjiang Bay continuum.

at 270 and 355 nm and one emission maximum at 448 nm, spanning the region of both peak A and peak C, characteristic of UVC and UVA humic fluorophores (Coble, 2007). These components, primarily C1 and C2, are initially considered terrestrial-derived humic-like fluorophores (Coble, 2007), widely distributed in land-ocean interface, strongly associated with soil organic materials and microbial activities (Guo et al., 2014; Li et al., 2019b). C3, with excitation/emission maxima at 305/392 nm, originally identified as a marine-derived humic-like component, is also prevalent across various natural aquatic ecosystems. Biological activities (e.g., microbial activities, phytoplankton production) have been demonstrated to the primary autochthonous sources of C3 in seawater (Yamashita et al., 2008; Romera-Castillo et al., 2010). C4, displaying excitation/emission maxima at 275/340 nm, represents a

protein-like component consistent with tryptophan-like peak T (Coble, 2007). It is indicative of autochthonous DOM production and anthropogenic input (Yamashita and Tanoue, 2003; Guo et al., 2014; Yamashita et al., 2015). Comparisons with the OpenFluor database confirmed that four FDOM components in this study were consistent with PARAFAC-derived components from previous studies (Murphy et al., 2014). C1, C2 and C3 have 10, 17 and 28 pairs of match-ups, respectively, with a TCC of >0.95 for both excitation and emission ($TCC_{ex,em}$), suggesting a consistent presence across diverse environments (e.g., Li et al., 2015; Dainard et al., 2019; Gamrani et al., 2023). Protein-like C4, with $TCC_{ex,em}$ values exceeding 0.95, was matched in 103 previous studies, including various natural aquatic ecosystems (Yamashita et al., 2010; Gao and Gueguen, 2017), plankton community culture experiments (Stedmon and Markager, 2005; Bittar et al., 2015), and wastewater (Cohen et al., 2014; Huang et al., 2024).

3.3 Distributions of DOC and quantitative optical parameters

DOC concentrations in the Suixi Estuary-Zhanjiang Bay continuum displayed significant variability, ranging from 55.4 to 1235.9 μmol/L. The summer of 2021 recorded the highest mean concentration at 327.9 ± 232.0 μmol/L, while the lowest was in the spring of 2022 at 170.4 ± 62.7 μmol/L (Table 1). A statistically significant difference in DOC concentrations between surface and bottom waters was observed only in the summer of 2022 (*t*-test, p = 0.01), with higher averages in surface waters. The upper Suixi Estuary consistently showed the highest DOC concentrations, which decreased progressively towards the sea across all seasons. Notably high DOC levels were documented in the central region of Zhanjiang Bay during the summers of 2021 and 2022 (Figures 3A–E; Supplementary Figures S3A–E).

Strong positive correlations were found among CDOM absorption coefficients at various wavelengths (i.e., a_{254}, a_{280}, a_{300}, a_{325}, a_{350}, a_{355}, and a_{412}) in the continuum (r > 0.97, p< 0.0001, n = 195). Thus, for simplicity, this study focuses on the a_{350} results, which ranged from 0.42 m^{-1} to 7.32 m^{-1} (Table 1). The average a_{350} peaked in summer 2022 (3.28 ± 1.64 m^{-1}) and reached its minimum in spring 2022 (1.52 ± 1.21 m^{-1}), with significant difference noted in summer 2022 between surface and bottom waters (*t*-test, p = 0.003). The highest a_{350} values were consistently observed in the upper Suixi estuary, diminishing towards the sea throughout the year. (Figures 3F–J; Supplementary Figures S3F–J).

The intensities of three humic-like components (C1, C2 and C3) demonstrated strong correlations (r > 0.97, p< 0.0001, n = 195), ranging from 0.08-1.17 RU, 0.01-0.61 RU, and 0.02-0.55 RU, respectively. The peak mean intensity of C1 was recorded in autumn 2021 (0.53 ± 0.35 RU), with the lowest occurring in spring 2022 (0.31 ± 0.24 RU). Conversely, the highest mean intensities for C2 and C3 were observed in the summer of 2022, whereas their lowest values were noted in the summer of 2021 (Table 1). The protein-like C4 intensity ranged from 0.01 to 0.47 RU, peaking in winter 2021 (0.20 ± 0.09 RU) and showing the lowest value in summer 2021 (0.12 ± 0.05 RU). The significant differences between surface and bottom waters were detected only in summer 2022 for all components (*t*-test, p values ranging from 0.002 to 0.006). The intensities of three humic-like components (C1, C2, and C3) were strongly correlated with the a_{350} (r > 0.83, p< 0.0001, n = 195), exhibiting similar distribution patterns throughout the Suixi Estuary-Zhanjiang Bay continuum (Figures 3K–Y; Supplementary Figures S3K–Y). However, the intensities of protein-like C4 showed a positive correlation with DOC concentrations at each season (r: 0.58-0.95, p< 0.0001) and followed a similar distribution pattern across the continuum (Figures 3Z–AD; Supplementary Figures S3Z–AD).

3.4 Distributions of qualitative optical parameters

The spectral slope $S_{275\text{-}295}$ ranged from 12.9 to 22.7 μm^{-1}, showing a contrasting spatial distribution pattern compared to a_{350} (Figures 4A–E; Supplementary Figures S4A–E). The highest mean $S_{275\text{-}295}$ value occurred in summer 2021, while the lowest was noted in summer 2022. $SUVA_{254}$ values showed a broad range from 0.24 to 6.74 m^2/g C, peaking in autumn 2021, with the lowest values occurring in summers 2021 and 2022 (Table 1). Generally, $SUVA_{254}$ decreased towards the sea, except in autumn when significantly lower values were recorded in the central continuum (Figures 4F–J; Supplementary Figures S4F–J). HIX varied from 0.88 to 6.22, decreasing from the upper estuary to lower bay, with the highest mean value in summer 2022 (Figures 4K-O; Supplementary Figures S4K–O). Conversely, BIX values ranged from 0.79 to 1.83, gradually increasing towards the sea and recording the lowest mean value in summer 2022 (Table 1; Figures 4P-T; Supplementary Figures S4P–T). FI values, varying from 2.41 to 2.61, showing the minimal spatial and temporal variation (Figures 4U–Y; Supplementary Figures S4U–Y). No significant differences were found between surface and bottom water for all DOM qualitative parameters (p > 0.05).

4 Discussion

4.1 Seasonal variability of freshwater and seawater DOM endmembers

Seasonal variations in riverine DOM endmember are well-documented across different climate regions (Guo et al., 2011; Li et al., 2019b; Yang et al., 2019). These variations affect the dynamics of riverine DOM in estuarine and coastal environments (Fichot and Benner, 2014) and introduce uncertainty (~30%) in quantifying global riverine DOM fluxes (Liu et al., 2024). In the Suixi estuary-Zhanjiang Bay continuum, freshwater DOC endmember values ranged from 355 to 708 μmol/L, peaking in autumn 2021 and reaching their lowest in winter 2021 (Table 2). A strong positive correlation was found between DOC and humic-like C1 in freshwater endmembers (r = 0.88, p = 0.05, n = 5). Freshwater endmembers with high levels of DOC and C1 typically exhibited low $S_{275\text{-}295}$ and BIX, alongside high HIX (Table 2), suggesting a predominance of terrestrial organic materials with high

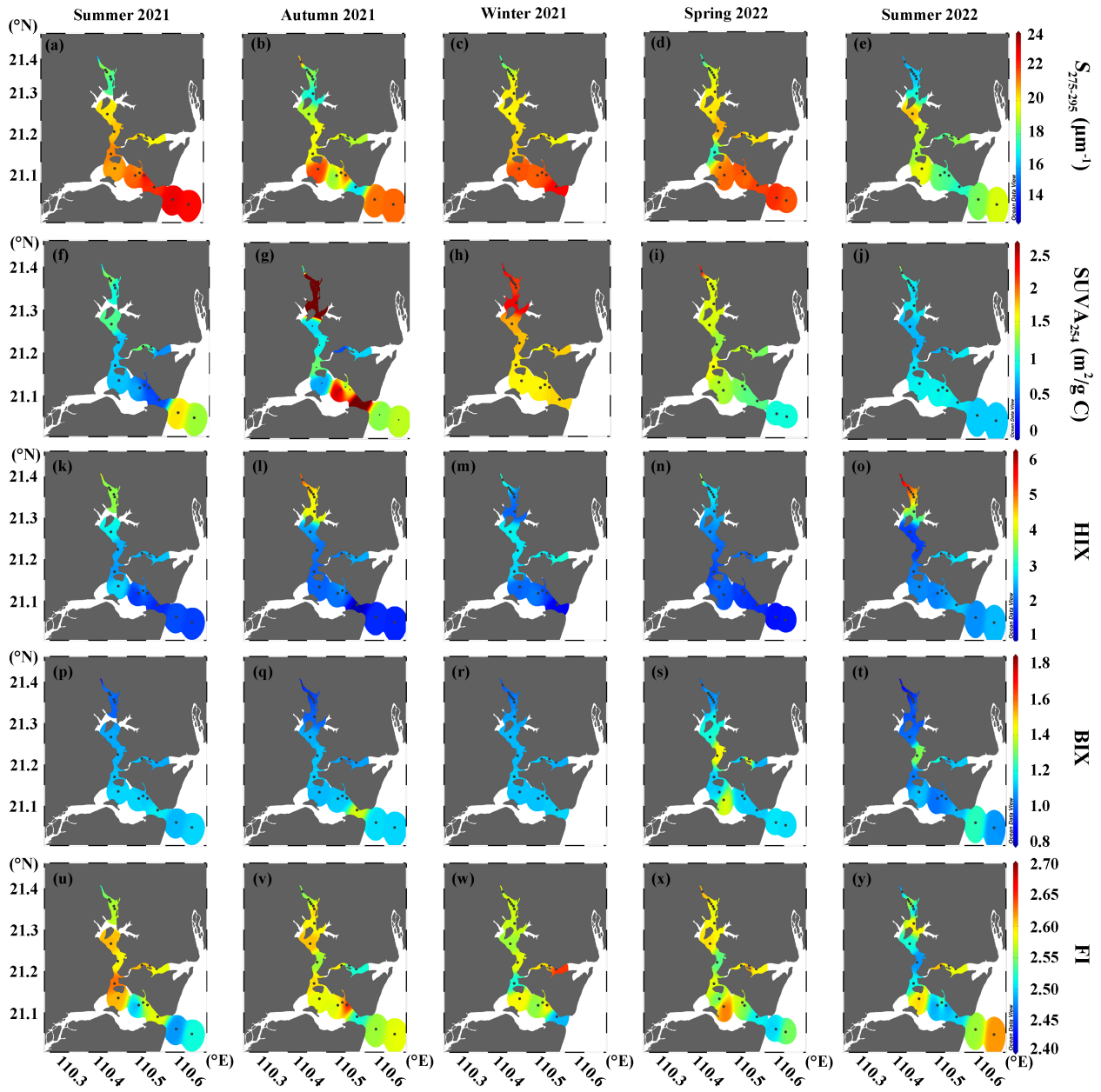

FIGURE 4
Seasonal distributions of **(A–E)** $S_{275-295}$, **(F–J)** $SUVA_{254}$, **(K–O)** HIX, **(P–T)** BIX, and **(U–Y)** FI in surface waters of the Suixi Estuary-Zhanjiang Bay continuum.

humification degrees, low freshness, and high molecular weights in the Suixi River DOM pool (Hansen et al., 2016; Huguet et al., 2009; Helms et al., 2008). Protein-like components constituted only 10-18% of the total fluorescence intensity in freshwater DOM pool (Table 2), underscoring the dominance of natural terrestrial inputs. This is consistent with the high-productivity tropical forests and wetlands surrounding the Suixi River watershed (Zhong et al., 2022). Soil leaching and erosion, driven by high annual precipitation (~1800 mm, Chen et al., 2021), are likely the main contributors to the river's high terrigenous DOM content. This is supported by a strong correlation between the freshwater DOC and C1 endmember values and 15-d cumulative precipitation prior to each cruise ($r > 0.96$, $p < 0.05$, $n = 4$), except for spring 2022. A short residence time of DOM in soil environments, driven by high precipitation, may limit its mineralization, thereby facilitating rapid transport to the river and maintaining high DOC levels in the riverine endmember.

In seawater endmembers, DOM levels were consistently lower (74-91%) than in freshwater endmembers. Differences in CDOM and $FDOM_H$ (89-91%) being more pronounced compared to DOC (78 ± 12%) and $FDOM_P$ (74 ± 2.5%). This suggests decreased aromaticity and increased bioavailability, as indicated by lower $SUVA_{254}$ and higher H/P values (Table 2). The seawater endmembers were mainly influenced by the West-Guangdong

TABLE 2 Seasonal variations in DOM and nutrient endmember values for freshwater and seawater in the Suixi Estuary-Zhanjiang Bay continuum.

Endmember	Season	Salinity	DOC (μmol/L)	a_{350} (m^{-1})	C1 (RU)	C2 (RU)	C3 (RU)	C4 (RU)	$SUVA_{254}$ (m^2/g C)	H/P	DIN (μmol/L)	SRP (μmol/L)	N/P
Fresh water	Summer 2021	0	553.74	7.53	1.17	0.51	0.38	0.28	1.80	7.36	194.60	3.52	55.28
	Autumn 2021	0	707.65	6.86	1.59	0.61	0.55	0.34	1.58	8.09	231.98	5.77	40.21
	Winter 2021	0	355.38	5.52	1.10	0.47	0.45	0.45	2.26	4.49	263.87	3.22	82.06
	Spring 2022	0	635.07	6.42	1.31	0.54	0.56	0.46	1.55	5.24	188.18	5.37	35.03
	Summer 2022	0	435.27	7.49	1.15	0.63	0.57	0.28	2.56	8.39	200.84	5.14	39.09
Seawater	Summer 2021	30.72	77.72	0.61	0.12	0.04	0.04	0.07	1.67	2.86	3.23	0.18	17.93
	Autumn 2021	32.16	75.58	0.54	0.11	0.03	0.03	0.10	1.50	1.70	2.18	0.06	36.36
	Winter 2021	30.15	116.50	0.91	0.21	0.08	0.07	0.13	1.61	2.77	6.78	0.79	8.63
	Spring 2022	30.06	103.43	0.68	0.13	0.05	0.04	0.11	1.40	2.00	11.35	0.09	126.1
	Summer 2022	32.48	162.03	1.01	0.08	0.03	0.03	0.07	1.05	2.00	0.90	0.04	22.38

The station with lowest salinity each season was designated as low-salinity endmember. The seawater endmember was identified as the station with highest salinity for each season. For summer 2021, the lowest recorded salinity was zero, indicating that the low-salinity endmember values represent the freshwater endmember. Freshwater endmember values for quantitative parameters (DOC, a_{350}, C1, C2, C3, C4, DIN, and SRP) during autumn 2021, winter 2021, spring 2022, and summer 2022—recorded for low-salinity endmembers with a salinity greater than 0—were calculated as the intercepts of linear fits between these low-salinity and seawater endmembers. The freshwater endmember values for $SUVA_{254}$ and N/P in these seasons were derived from the theoretical freshwater endmembers for DOC, a_{254}, DIN, and SRP.

10.3389/fmars.2024.1511427

Coastal Current (WGCC) and tidal activities (Ding et al., 2017; Huang et al., 2021; Lao et al., 2022), contributing to modest variations in seawater salinity endmember values in this study (30.06-32.48, Table 2). In comparison, the variation in DOM within seawater endmembers was pronounced, contrasting with other systems, such as Pearl River and Jiulong River estuaries, which showed minimal variations in their seawater endmembers (Guo et al., 2007, 2011; Li et al., 2019b). In summer 2021, an intensified WGCC transported terrigenous materials from rivers in western Guangdong (e.g., Peral River, Moyang River, and Jian River), which contributed to the relatively low salinity but high H/P and $SUVA_{254}$ values in seawater endmember (Table 2). Conversely, summer 2022 saw the highest DOC and lowest $SUVA_{254}$ values in seawater endmembers, indicative of significant contributions from primary production, as evidenced by depleted levels of DIN and SRP (Table 1). The lack of correlation between salinity and DOM within seawater endmembers ($p > 0.05$) further highlights the importance of *in situ* biogeochemical transformations in shaping DOM within seawater endmembers. Seasonal variability in both freshwater and seawater DOM endmembers, driven by natural and anthropogenic factors, delineates the complex dynamics of DOM in the Suixi Estuary-Zhanjiang Bay continuum. With reduced runoff and enhanced dredging activity, salinity in the Suixi Estuary-Zhanjiang Bay continuum has risen by 18% over the past two decades (Lao et al., 2022), undoubtedly altering the DOM budget and transformation in the continuum and emphasizing the need for continued research.

4.2 Mixing behaviors of DOM in the Suixi Estuary-Zhanjiang Bay continuum

The transport of dissolved organic matter (DOM) from rivers to the ocean, especially through estuaries and coastal bays, involves complex physicochemical and biogeochemical processes that significantly alter the composition, reactivity, flux, and fate of riverine DOM as it reaches the ocean shelf (Raymond and Spencer, 2015; Spencer and Raymond, 2024).These transformations can be assessed through the relationships between DOM and salinity gradients (Huguet et al., 2009; Fellman et al., 2011; Guo et al., 2011; Vidal et al., 2023). Our findings indicate significant linear decreases in DOC, a_{350} and FDOM intensities with increasing salinity ($p< 0.05$), suggesting that conservative mixing of freshwater and seawater is the primary factor shaping the distribution of DOM in the Suixi Estuary-Zhanjiang Bay continuum (Figure 5). However, the R^2 values for these linear fits varied substantially across different DOM parameters and seasons, highlighting the complexity of the interactions. The linear fittings between $FDOM_H$ and salinity demonstrated the highest R^2 values (0.85-0.97 for C1, 0.86-0.98 for C2, and 0.83-0.96 for C3), followed by those between a_{350} and salinity (0.46-0.99), between $FDOM_P$ and salinity (0.22-0.89), and between DOC and salinity (0.25-0.92). Salinity explained over 83% of the variation in $FDOM_H$, indicating that these components were dominated by the conservative mixing of freshwater and seawater endmembers. Non-conservative processes such as flocculation (Guo et al., 2007; Asmala et al., 2014), photobleaching (Moran et al., 2000; Catalá et al., 2013), and microbial activities (Klinkhammer et al., 2000; Yang et al., 2019) appeared to have a relatively small impact on their distributions across all seasons. Conservative mixing accounted for most of the variability in CDOM distribution during winter 2021 and in spring and summer 2022 ($R^2 \geq 0.86$) but explained only half of the variability in CDOM in autumn 2021 ($R^2 = 0.46$). DOC and protein-like C4, proxies for labile DOM produced by primary production and degraded by microbes but relatively resistant to photobleaching (Yang et al., 2019), exhibited the expected weakest correlations with salinity in the Suixi Estuary-Zhanjiang Bay continuum (Figure 5). This was particularly noticeable in autumn 2021 and summer 2022 ($0.22 \leq R^2 \leq 0.63$), periods characterized by higher Chl-a concentrations (Figure 3; Supplementary Figure S3). These diverse mixing behaviors among different DOM components and across seasons demonstrate the substantial modification riverine DOM undergoes when passing through estuarine environments (Spencer and Raymond, 2024), influencing the flux and fate of allochthonous DOM entering the northern SCS.

4.3 Seasonal variations of non-conservative DOM in the Suixi Estuary-Zhanjiang Bay continuum

Beyond assessing DOM behavior through correlations with salinity, a multiple endmember mixing model provides insights into both conservative and nonconservative processes impacting the DOM pool in estuarine and coastal environments (Dittmar et al., 2001; Ya et al., 2015; Jiang et al., 2017). In the Suixi Estuary-Zhanjiang Bay continuum, freshwater discharge from the Suixi River and seawater intrusion from the adjacent northern SCS are the primary allochthonous DOM sources (Lao et al., 2022). Other potential sources, such as submarine groundwater discharge, atmospheric deposition, and sediment release are considered limited based on dual water isotopes (Lao et al., 2023a) and DOM-salinity relationships (Figure 5). Thus, a two-endmember mixing model was utilized in this study:

$$f_{FW} \times Sal_{FW} + f_{SW} \times Sal_{SW} = Sal_{obs} \quad (2)$$

$$f_{FW} \times M_{FW} + f_{SW} \times M_{SW} + \Delta M = M_{obs} \quad (3)$$

Here, f_{FW} and f_{SW} represent the fractions of freshwater and seawater endmembers in a given water parcel, respectively, with Sal_{FW} and Sal_{SW} denoting their salinity values. Sal_{obs} and M_{obs} refer to the observed salinity and DOM parameters. M_{FW} and M_{SW} represent the DOM values of the respective endmember (Table 2). ΔM denotes nonconservative changes in DOM, with positive ΔM values indicating additions to the DOM pool. The relative change in M due to nonconservative processes (%) was calculated as the ratio of ΔM to M_{obs}. To discuss the effect of nutrients on the nonconservative processes of DOM, ΔDIN and ΔSRP were also calculated using this method.

ΔDOC ranged from -30 to 685 μmol/L in summer 2021 (163 ± 168 μmol/L), -364 to 114 μmol/L in autumn 2021 (-74 ± 160

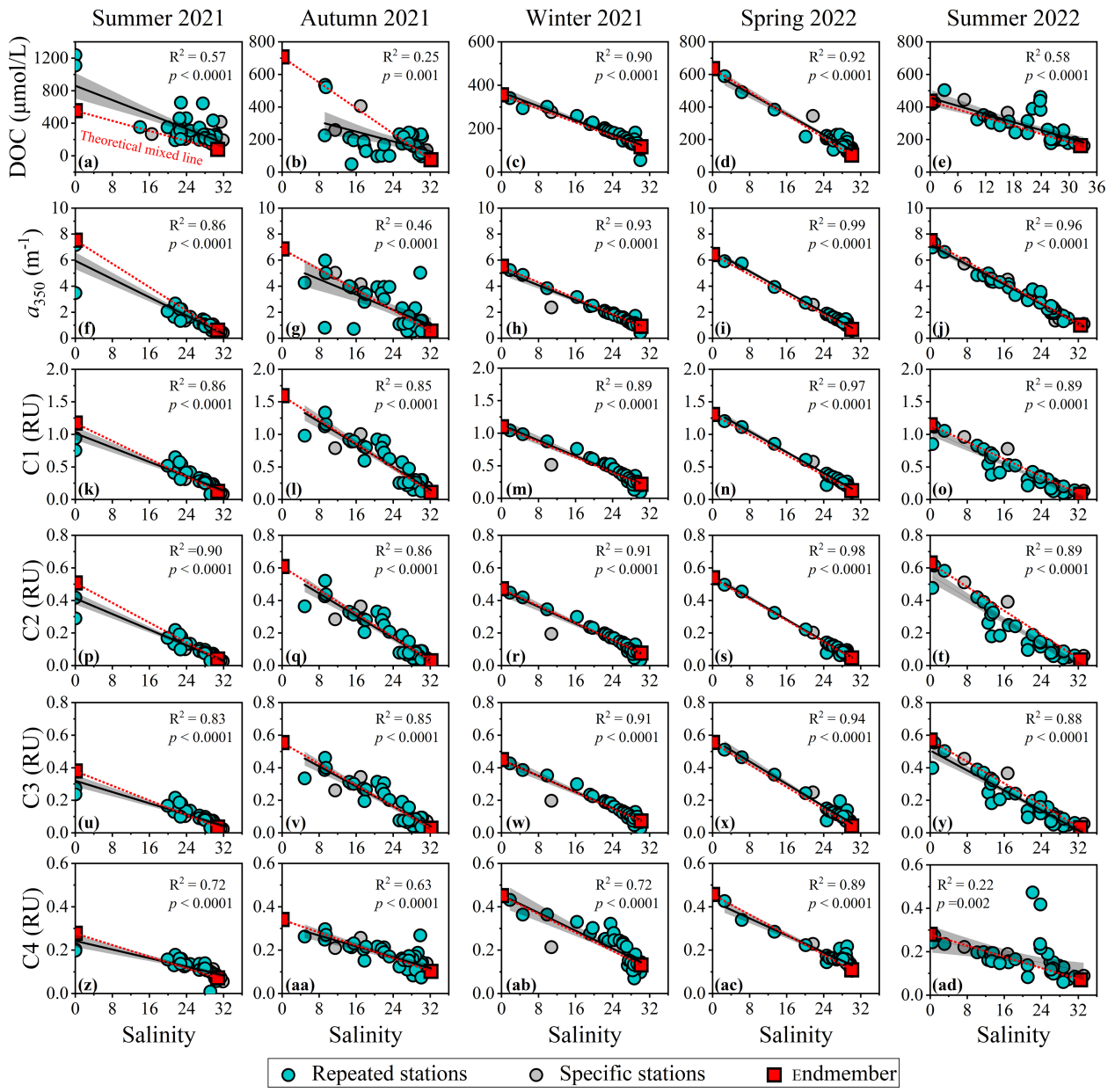

FIGURE 5
Seasonal variations in the relationships between **(A–E)** DOC, **(F–J)** a_{350}, and **(K–AD)** intensities of four FDOM components with salinity across the Suixi Estuary-Zhanjiang Bay continuum. Black solid lines and gray shadows illustrate the linear fits and their 95% confidence bands, respectively. Red dotted lines represent the theoretical mixing lines between freshwater and seawater endmembers.

μmol/L), -116 to 56 μmol/L in winter 2021 (12 ± 17 μmol/L), -61 to 94 μmol/L in spring 2022 (22 ± 30 μmol/L), and -39 to 227 μmol/L (25 ± 65 μmol/L), respectively. Significant additions of DOC (*t*-test, $p< 0.05$) were common but varied greatly across seasons: summer 2021 (102 ± 95%), winter 2021 (7.5 ± 11.7%), spring 2022 (18.0 ± 19.0%), and summer 2022 (10.7 ± 26.9%), despite the overall conservative behaviors of DOC during these seasons ($p< 0.0001$, Figures 5A, C–E). Although the mean ΔDOC was not significantly different from zero in autumn 2021 ($p > 0.05$, Figure 6A), negative ΔDOC values (-177 ± 100 μmol/L) were found in the low-salinity waters (salinity< 25, $p< 0.0001$) and positive values in high-salinity waters (salinity > 25, $p = 0.002$), indicating remarkable DOC removal in the upper continuum (-50 ± 24%) and addition in the lower bay (25 ± 33%). Phytoplankton production was identified as the primary process responsible for the DOC addition. Positive relationships between ΔDOC and Chl-a in summer 2021 (r = 0.44, $p = 0.02$) and 2022 (r = 0.87, $p< 0.001$) support DOM accumulation during actively growing phytoplankton blooms (Søndergaard et al., 2000; Hoikkala et al., 2012; Liu et al., 2024). Maximum DOC addition occurred in area with medium-high salinity (20-30, Figures 5A, E), where nutrient inputs from urban sewage discharge (Zhang et al., 2021), extended water residence times (Cai et al., 2024), and warm temperatures favored phytoplankton blooms (maximum Chl-a > 10 μg/L in summer 2021 and 50 μg/L in summer 2022).

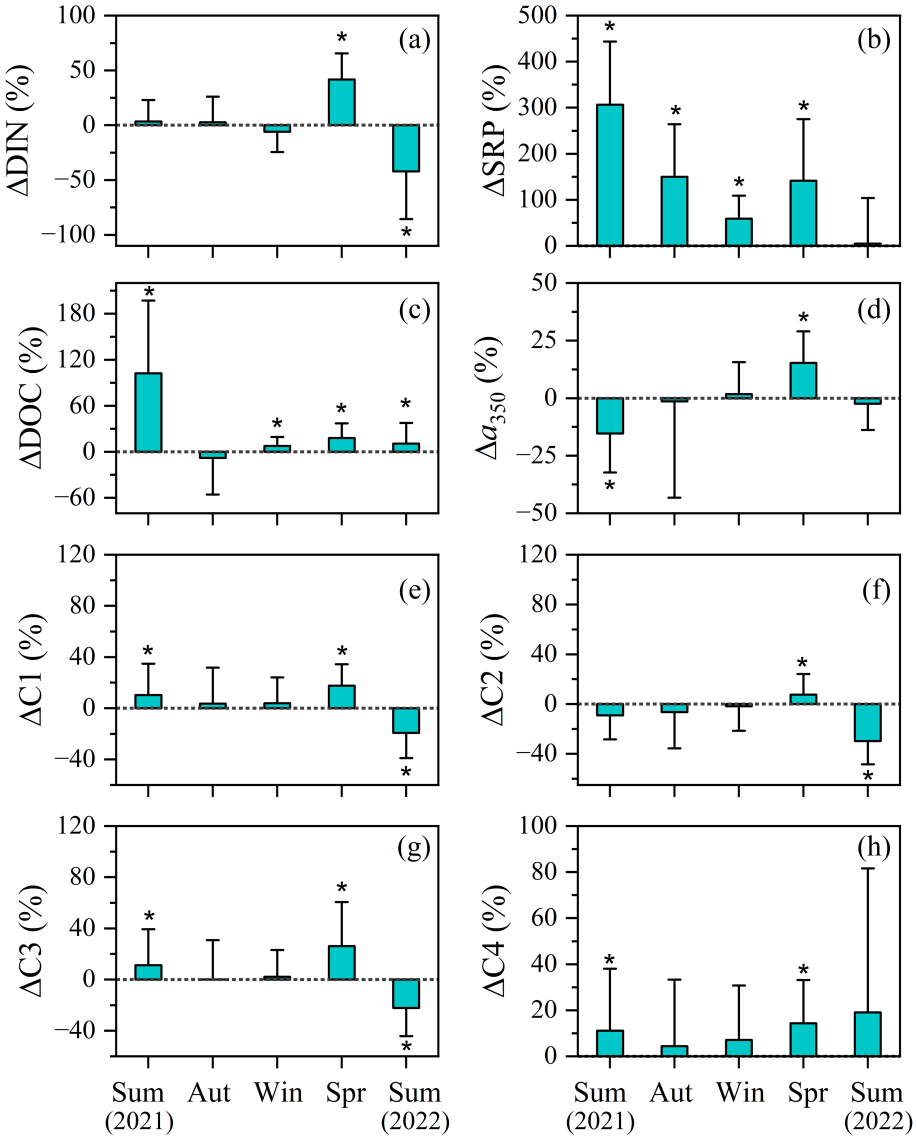

FIGURE 6
Seasonal comparison of proportions of nonconservative **(A)** DIN, **(B)** SRP, **(C)** DOC, **(D)** a_{350}, and **(E–H)** four FDOM components in the Suixi Estuary-Zhanjiang Bay continuum. An asterisk (*) indicates that the mean value is significantly different from zero at the 0.05 significance level.

Higher Chl-a levels in summer 2022 coincided with greater nutrient removals but did not result in as much DOC addition as in summer 2021 (Table 1, Figure 6), suggesting regulation by other biogeochemical processes. The bio-refractory $FDOM_H$, less directly influenced by primary production than DOC, could offer valuable insights. Substantial removals in $FDOM_H$ (-19 ± 20% for C1, -30 ± 19% for C2, -22 ± 22% for C3) were found in summer 2022 (Figures 6D–H), especially in the low salinity region (~ 13), suggesting potential flocculation of DOM in this season (McCallister et al., 2006; Asmala et al., 2014). Although the bulk DOC flocculates more slowly than humic fraction of DOM (Eckert and Sholkovitz, 1976), we speculate that this flocculation may partially offsets the enhanced DOC in summer 2022. Additionally, labile DOC from phytoplankton photosynthesis could have a priming effect on riverine terrigenous refractory DOM, facilitating its partial remobilization for microbial utilization (Bianchi, 2011; Jiao et al., 2011; Spencer and Raymond, 2024). This stimulated microbial degradation likely also contributes to the removal of $FDOM_H$ in the Suixi Estuary-Zhanjiang Bay continuum. In contrast, substantial addition of $FDOM_H$ (10 ± 25% for C1 and 11 ± 26% for C3) were observed in summer 2021, linked to the *in situ* production during microbial-mediated degradation of labile carbon, as evidenced by positive correlations between $\Delta FDOM_H$ and ΔDIN (r: 0.53-0.63, $p < 0.005$).

In spring, negative correlations were observed between ΔDOC and Chl-a (r = -0.45, $p = 0.009$), and between ΔC4 and Chl-a (r = -0.49, $p = 0.004$), suggesting DOC and $FDOM_P$ accumulated during declining algal blooms (Lønborg et al., 2009). Previous studies demonstrated that increased primary production facilitated rapid heterotrophic microbial degradation of labile organic matter, with particulate organic matter as the major substrate (Lao et al., 2023b). During the net-anabolic phase of heterotrophic microbial

communities, some traditionally defined labile DOM compounds could be released through extracellular release, protist grazing, and viral lysis, decreasing Chl-a and enhancing DOC and $FDOM_P$ levels (Kawasaki and Benner, 2006; Lønborg et al., 2009). Concurrently, the net-catabolic phase of microbial activities could release more bio-refractory compounds such as CDOM and $FDOM_H$ as the by-products (Xiao et al., 2022), contributing to their significant additions in spring 2022 (15 ± 13% for a_{350}, 18 ± 17% for C1, 8 ± 17% for C2, and 26 ± 34% for C3, Figure 6). This is supported by significant additions of DIN (14.3 ± 16.6 μmol/L, 39 ± 24%, Figure 6A) and SRP (0.59 ± 0.44 μmol/L, 123 ± 134%, Figure 6B), coupled with linear relationships between Δ values for $FDOM_H$ and nutrient and DO levels (e.g., ΔC1 vs. ΔDIN: r = 0.44, $p = 0.015$; ΔC1 vs. ΔSRP: r = 0.86, $p < 0.0001$; ΔC1 vs. DO: r = -0.69, $p < 0.0001$). These findings illustrate the prevalence of microbial-mediated transformation from labile biogenic particles to refractory DOM in spring 2022, accompanied by oxygen consumption and nutrient regeneration (Xiao et al., 2022). Precisely due to considerable contributions from both primary productivity and microbial transformation, DOM in spring 2022 in the continuum experienced extensive reworking, resulting in the highest fraction of bio-labile materials, lowest humification degree and molecular weight, and greatest freshness of any season (Table 1).

Unlike the visible removal of DOC occurred in the upper continuum during autumn 2021, CDOM and FDOM remained largely unaffected (Figure 5). This pattern suggests that riverine DOM was more efficiently consumed by heterotrophic microorganism, similar to summer 2022 (Bianchi, 2011; Zhuang et al., 2021). Microbial degradation was stimulated by locally produced labile DOC under the conditions of ample nutrients and favorable temperature (Tables 1, 2). Alongside gradual depletion of degradable riverine DOM toward the sea, positive ΔDOC emerges in the lower continuum (Figure 6), most likely resulting from phytoplankton bloom (Figure 2; Carlson and Hansell, 2015). The single-peak pattern of ΔDOC-Chl-a relationship in the lower continuum during autumn 2021 suggests an uncoupling of dissolved and particulate organic materials subjected to microbial decomposition, indicating preferential utilization of locally produced POM (Lao et al., 2023b). In winter 2021, characterized by the lowest river discharge and temperatures (Table 1; Figure 2), the estuarine DOM was the least dynamic, with no significant change in CDOM and FDOM levels ($p > 0.05$, Figure 6). This stability suggests minimal reworking of riverine DOM, aligning with observations from other seasonal estuaries (Li et al., 2019b; Gao et al., 2020). These findings highlight the substantial seasonal and interannual variations in estuarine DOM dynamics, driven by shifts in endmembers and influenced by both abiotic and biotic processes during water masses mixing (Bianchi, 2011; Vidal et al., 2023). The results underscore the necessity for high-frequency investigations to accurately track the transport and transformation of DOM from small tropical rivers to the coastal seas (Liu et al., 2024).

4.4 Export of riverine DOM by Suixi River and global perspective

The fluxes of DOM (i.e., DOC, CDOM, and FDOM) from Suixi River to the Zhangjiang Bay were estimated as follows (Guo et al., 2014; Li et al., 2019b):

$$F = Q \times C^{*} \quad (4)$$

Where F represents the flux of DOM, Q denotes the Suixi River discharge, and C^{*} represents the freshwater endmember values of DOM (Table 2). Annual riverine DOM fluxes were calculated by summing the DOM fluxes from four seasons, using the average of the two summer fluxes as one component. Specifically, the annual DOM flux of the Suixi River was calculated as follows: 3.4×10^{10} g C/yr for DOC, 3.5×10^{10} m^2/yr for a_{350}, 6.3×10^{9} RU m^3/yr for C1, 2.8×10^{9} RU m^3/yr for C2, 2.5×10^{9} RU m^3/yr for C3, and 1.7×10^{9} RU m^3/yr for C4. In summer, the Suixi River accounted for 56% of the annual water discharge, but contributed only 47-49% of the annual DOC and $FDOM_P$ fluxes, while providing 59 ± 0.2% of the annual CDOM flux and 51-56% of the annual $FDOM_H$ flux. This is attributed to stronger soil leaching and washing processes during summer, which mobilize more refractory terrigenous DOM materials into the Suixi Estuary-Zhanjiang Bay continuum, highlighting the seasonal variation in the composition and flux of riverine DOM transported by small tropical rivers.

DOC concentrations in the Suixi River are moderately high compared to other Chinese and global rivers (Figure 7A, Raymond and Spencer, 2015; Wang et al., 2022; Spencer and Raymond, 2024). These concentrations are only exceeded by the pan-Arctic Rivers, which range from 364-805 μmol/L (Stedmon et al., 2011), and rivers significantly affected by anthropogenic inputs, such as the Hai River at ~868 μmol/L (Xia and Zhang, 2011). However, the DOC levels are comparable to those found in major tropical rivers like the Amazon and Orinoco, as well as North American rivers (Spencer et al., 2013; Raymond and Spencer, 2015). In contrast, the Suixi River exhibits significantly higher concentrations than other Chinese subtropical and temperate rivers including the Yangtze River (116-174 μmol/L, Guo et al., 2014), Pearl River (82-124 μmol/L, Li et al., 2019b), Min River (88-110 μmol/L, Yang et al., 2019), Jiulong River (132-186 μmol/L, Guo et al., 2011), and mountainous Taiwan rivers (32-139 μmol/L, Yang et al., 2013). However, the CDOM levels in Suixi River (a_{350}-based, 6.76 ± 0.83 m^{-1}) align closely with the global average (6.18 ± 5.16 m^{-1}, Figure 7A), resulting in the noticeable deviations from the lineal DOC-a_{350} relationship observed across global 52 rivers (Figure 7A).

In terms of DOM quality, the $SUVA_{350}$ values for the Suixi River (0.48 ± 0.12 m^2/g C) fall within the low to moderate range globally (0.64 ± 0.23 m^2/g C, Figure 7B). These values were notably lower than those found in large tropical rivers (0.92 ± 0.13 m^2/g C), North American rivers (0.71 ± 0.26 m^2/g C), and pan-Arctic rivers (0.62 ± 0.12 m^2/g C), yet similar to other Chinese rivers (0.47 ± 0.19 m^2/g C, Supplementary Table S2). From a global perspective, peak $SUVA_{350}$ values for river endmembers were observed at moderate water yields (m/yr, Figure 7B). A reasonable explanation is that larger water yield facilitates stronger interactions between river and soil, which in turn promote the release of soil organic carbon enriched in reworked CDOM. Once the soil reworked organic carbon is sufficiently mobilized, the increased water yield can enhance the contribution of labile carbon from net primary production to riverine DOM pool (Tromboni et al., 2022), as reflected by decreased $SUVA_{350}$ values for river water endmembers (Figure 7B). The ongoing changes in climate (e.g.,

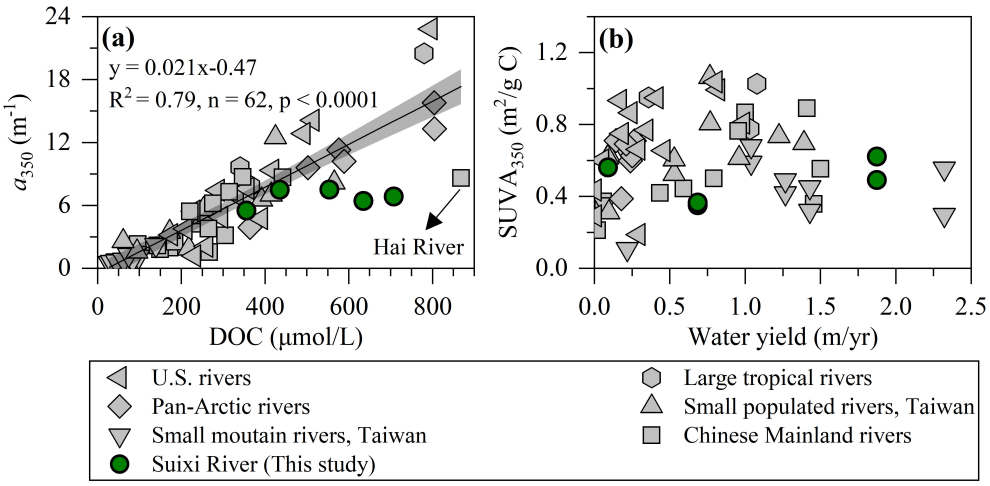

FIGURE 7
Relationships between **(A)** a_{350} and DOC, and between **(B)** $SUVA_{350}$ and the ratio of water discharge to watershed area for global river endmembers. Black line and gray shadow in panel a represent the linear fit and confidence band (95%) for a total of 52 river endmembers in the globe, respectively. Data are listed in Supplementary Table S2.

temperature and precipitation) and intensifying human activities (e.g., land utilization, dam construction) continue to affect the water yields of global tropical rivers (Wu et al., 2023; Vystavna et al., 2024), undoubtedly exert dynamic of riverine DOM composition entering the sea (Liu et al., 2022). Despite similar $SUVA_{350}$ values, both the DOC yield (21.9 g C/m^2/yr) and CDOM yield (a_{350}-based, 21.9 yr^{-1}) of the Suixi River far exceed those of other Chinese rivers (2.68 ± 4.46 g C/m^2/yr and 2.78 ± 4.08 yr^{-1}, respectively). This uncoupling is largely attributed to high watershed productivity and strong soil leaching in the Suixi River, compared to other subtropical and temperate Chinese rivers, which are affected by a low abundance of aged and leached soil organic matter, dam construction, and rapid wetlands reduction due to anthropogenic exploitation (Guo et al., 2014). This exceptionally high DOC yield from the Suixi River, more than twice the highest recorded yield from the large tropical Fly River (~8.6 g C/m^2/yr, Raymond and Spencer, 2015), highlights the critical role of small, tropical rivers in estuarine and coastal carbon cycling and the need to consider these smaller systems in broader ecological and biogeochemical studies.

5 Conclusion

This study reveals the complex dynamics at the tropical river-sea interface of the Suixi Estuary-Zhanjiang Bay continuum, highlighting the significant role of small tropical watersheds in global carbon cycling. Our analysis from summer 2021 to summer 2022 encompassed DOC, CDOM, and FDOM, showing pronounced seasonal variations. DOC in freshwater endmember peaked in autumn 2021, driven largely by terrestrial inputs as evidenced by strong correlations with $FDOM_H$ and enhanced by soil erosion and leaching that correlate with precipitation. Conversely, DOC in seawater endmember peaked in summer 2022, enriched in $FDOM_P$ and influenced by the West-Guangdong Coastal Current alongside *in situ* primary production.

Our findings indicate that while conservative mixing of freshwater and seawater predominantly influences DOM distribution within the continuum, significant non-conservative modifications occur through flocculation, phytoplankton production, and microbial transformation. These alterations vary across seasons, affecting the DOM's qualitative and quantitative characteristics. Despite the Suixi River accounting for a substantial portion of the annual water discharge (56%), its contribution to annual DOM fluxes (47-59%) does not proportionately reflect its output, primarily due to intense seasonal soil leaching that mobilizes more refractory terrigenous DOM. This phenomenon results in remarkably high DOC and CDOM yields, substantially exceeding those recorded for other Chinese rivers and even global peak yields like the tropical Fly River.

Our analysis also revealed a distinct single-peak pattern between the $SUVA_{350}$ values for river endmembers and water yield, based on a global dataset. This pattern suggests that maximum mobilization of soil-derived refractory organic carbon occurs at moderate water yields. Beyond this peak, refractory soil carbon contributions diminish while labile carbon input from net primary production increases, highlighting the complex interplay between hydrological dynamics and carbon cycling processes. The study demonstrates that the Suixi River, like other small tropical rivers, plays a crucial role in the estuarine and coastal carbon budget. Moving forward, integrating small tropical watershed data into global carbon models is essential to enhance the accuracy of carbon budget estimations.

Data availability statement

The original contributions presented in the study are included in the article/Supplementary Material. Further inquiries can be directed to the corresponding author.

Author contributions

PL: Formal analysis, Investigation, Visualization, Writing – original draft. KJ: Investigation, Writing – original draft. QT: Investigation, Writing – original draft. FC: Writing – review & editing. RJ: Writing – review & editing. CW: Conceptualization, Funding acquisition, Methodology, Writing – original draft, Writing – review & editing.

Funding

The author(s) declare financial support was received for the research, authorship, and/or publication of this article. This work was funded by the Guangdong Basic and Applied Basic Research Foundation (2022A1515110946), the open grant from Guangxi Key Laboratory of Beibu Gulf Marine Resources, Environment and Sustainable Development (MRESD-2022-B01), and the Tropical Ocean Environment in Western Coastal Waters Observation and Research Station of Guangdong Province (2024B1212040008).

Conflict of interest

The authors declare that the research was conducted in the absence of any commercial or financial relationships that could be construed as a potential conflict of interest.

Generative AI statement

The author(s) declare that no Generative AI was used in the creation of this manuscript.

Publisher's note

Supplementary material

The Supplementary Material for this article can be found online at: https://www.frontiersin.org/articles/10.3389/fmars.2024.1511427/full#supplementary-material

References

Asmala, E., Bowers, D. G., Autio, R., Kaartokallio, H., and Thomas, D. N. (2014). Qualitative changes of riverine dissolved organic matter at low salinities due to flocculation. *J. Geophysical Research-Biogeosciences* 119, 1919–1933. doi: 10.1002/2014JG002722

Bauer, J. E., and Bianchi, T. S. (2011). "Dissolved organic carbon cycling and transformation," in *Treatise on Estuarine and Coastal Science, 5* (Amsterdam, Netherlands: Academic Press, Waltham), 7–67.

Bauer, J. E., Cai, W. J., Raymond, P. A., Bianchi, T. S., Hopkinson, C. S., and Regnier, P. A. G. (2013). The changing carbon cycle of the coastal ocean. *Nature* 504, 61–70. doi: 10.1038/nature12857

Bianchi, T. S. (2011). The role of terrestrially derived organic carbon in the coastal ocean: A changing paradigm and the priming effect. *Proc. Natl. Acad. Sci.* 108, 19473–19481. doi: 10.1073/pnas.1017982108

Bittar, T. B., Vieira, A. A. H., Stubbins, A., and Mopper, K. (2015). Competition between photochemical and biological degradation of dissolved organic matter from the cyanobacteria Microcystis aeruginosa. *Limnology Oceanography.* 60, 1172–1194. doi: 10.1002/lno.10090

Cai, S., Lao, Q., Cai, M., Silva, D. P. T. T., Lu, X., Zhou, X., et al. (2024). Water residence time controls seasonal nitrous oxide budget in a semi-enclosed bay: Insights from an improvement estimation method. *Mar. Pollut. Bull.* 206, 116701. doi: 10.1016/j.marpolbul.2024.116701

Carlson, C. A., and Hansell, D. A (2015). "Chapter 3 - DOM sources, sinks, reactivity, and budgets," in *Biogeochemistry of marine dissolved organic matter, 2nd ed.* Eds. D. A. Hansell and C. A. Carlson (Academic Press, Boston), 65–126.

Carlson, C. A., Liu, S., Stephens, B. M., and Chance, J. (2024). "Chapter 5 - DOM production, removal, and transformation processes in marine systems," in *Biogeochemistry of Marine Dissolved Organic Matter, 3rd ed.* (Amsterdam, Netherlands: Academic Press), 137–246.

Carpenter, J. H. (1965). The Chesapeake bay institute technique for the winkler dissolved oxygen method. *Oceanography* 10, 141–143. doi: 10.4319/lo.1965.10.1.0141

Catalá, T. S., Mladenov, N., Echevarría, F., and Reche, I. (2013). Positive trends between salinity and chromophoric and fluorescent dissolved organic matter in a seasonally inverse estuary. *Estuar. Coast. Shelf Sci.* 133, 206–216. doi: 10.1016/j.ecss.2013.08.030

Chen, R. F., and Gardner, G. B. (2004). High-resolution measurements of chromophoric dissolved organic matter in the Mississippi and Atchafalaya River plume regions. *Mar. Chem.* 89, 103–125. doi: 10.1016/j.marchem.2004.02.026

Chen, F., Huang, C., Lao, Q., Zhang, S., Chen, C., Zhou, X., et al. (2021). Typhoon control of precipitation dual isotopes in Southern China and its palaeoenvironmental implications. *J. Geophysical Research: Atmospheres* 126, e2020JD034336. doi: 10.1029/2020JD034336

Coble, P. G. (2007). Marine optical biogeochemistry: The chemistry of ocean color. *Chem. Rev.* 107, 402–418. doi: 10.1021/cr050350+

Cohen, E., Levy, G. J., and Borisover, M. (2014). Fluorescent components of organic matter in wastewater: Efficacy and selectivity of the water treatment. *Water Res.* 55, 323–334. doi: 10.1016/j.watres.2014.02.040

Cory, R. M., and McKnight, D. M. (2005). Fluorescence spectroscopy reveals ubiquitous presence of oxidized and reduced quinones in dissolved organic matter. *Environ. Sci. Technol.* 39, 8142–8149. doi: 10.1021/es0506962

Dai, M., Su, J., Zhao, Y., Hofmann, E. E., Cao, Z., Cai, W., et al. (2022). Carbon fluxes in the coastal ocean: synthesis, boundary processes, and future trends. *Annu. Rev. Earth Planetary Sci.* 50, 593–626. doi: 10.1146/annurev-earth-032320-090746

Dainard, P. G., Guéguen, C., Yamamoto-Kawai, M., Williams, W. J., and Hutchings, J. K. (2019). Interannual variability in the absorption and fluorescence characteristics of dissolved organic matter in the Canada basin polar mixed waters. *J. Geophys Res: Oceans* 124, 5258–5269. doi: 10.1029/2018JC014896

Ding, Y., Bao, X., Yao, Z., Zhang, C., Wan, K., Bao, M., et al. (2017). A modeling study of the characteristics and mechanism of the westward coastal current during summer in the northwestern South China Sea. *Ocean Sci. J.* 52, 11–30. doi: 10.1007/s12601-017-0011-x

Dittmar, T., Lara, R. J., and Kattner, G. (2001). River or mangrove? Tracing major organic matter sources in tropical Brazilian coastal waters. *Mar. Chem.* 73, 253–271. doi: 10.1016/S0304-4203(00)00110-9

Eckert, J. M., and Sholkovitz, E. R. (1976). The flocculation of iron, aluminium and humates from river water by electrolytes. *Geochim Cosmochimica Acta* 40, 847–848. doi: 10.1016/0016-7037(76)90036-3

Fellman, J. B., Petrone, K. C., and Grierson, P. F. (2011). Source, biogeochemical cycling, and fluorescence characteristics of dissolved organic matter in an agro-urban estuary. *Limnology Oceanography*. 56, 243–256. doi: 10.4319/lo.2011.56.1.0243

Fichot, C. G., and Benner, R. (2014). The fate of terrigenous dissolved organic carbon in a river-influenced ocean margin. *Global Biogeochemical Cycles* 28, 300–318. doi: 10.1002/2013GB004670

Gamrani, M., Eert, J., Williams, W. J., and Gueguen, C. (2023). A river of terrestrial dissolved organic matter in the upper waters of the central Arctic Ocean. *Deep-Sea Res. Part I-Oceanographic Res. Papers* 196,196. doi: 10.1016/j.dsr.2023.104016

Gao, L., Gao, Y., Song, S., and Zhang, F. (2020). Non-conservative behavior of dissolved organic carbon in the Changjiang (Yangtze River) Estuary and the adjacent East China Sea. *Continental Shelf Res.* 197, 197. doi: 10.1016/j.csr.2020.104084

Gao, Z., and Gueguen, C. (2017). Size distribution of absorbing and fluorescing DOM in Beaufort Sea, Canada Basin. *Deep-Sea Res. Part I-Oceanographic Res. Papers* 121, 30–37. doi: 10.1016/j.dsr.2016.12.014

García-Martín, E. E., Sanders, R., Evans, C. D., Kitidis, V., Lapworth, D. J., Rees, A. P., et al. (2021). Contrasting estuarine processing of dissolved organic matter derived from natural and human-impacted landscapes. *Global Biogeochem Cycles* 35, 35. doi: 10.1029/2021GB007023

Guo, W., Stedmon, C. A., Han, Y., Wu, F., Yu, X., and Hu, M. (2007). The conservative and non-conservative behavior of chromophoric dissolved organic matter in Chinese estuarine waters. *Mar. Chem.* 107, 357–366. doi: 10.1016/j.marchem.2007.03.006

Guo, W., Yang, L., Hong, H., Stedmon, C. A., Wang, F., Xu, J., et al. (2011). Assessing the dynamics of chromophoric dissolved organic matter in a subtropical estuary using parallel factor analysis. *Mar. Chem.* 124, 125–133. doi: 10.1016/j.marchem.2011.01.003

Guo, W., Yang, L., Zhai, W., Chen, W., Osburn, C. L., Huang, X., et al. (2014). Runoff-mediated seasonal oscillation in the dynamics of dissolved organic matter in different branches of a large bifurcated estuaryThe Changjiang Estuary. *J. Geophysical Research-Biogeosciences* 119, 776–793. doi: 10.1002/2013JG002540

Hansen, A. M., Kraus, T. E. C., Pellerin, B. A., Fleck, J. A., Downing, B. D., and Bergamaschi, B. A. (2016). Optical properties of dissolved organic matter (DOM): Effects of biological and photolytic degradation. *Limnology Oceanography* 61, 1015–1032. doi: 10.1002/lno.10270

Helms, J. R., Stubbins, A., Ritchie, J. D., Minor, E. C., Kieber, D. J., and Mopper, K. (2008). Absorption spectral slopes and slope ratios as indicators of molecular weight, source, and photobleaching of chromophoric dissolved organic matter. *Limnology Oceanography* 53, 955–969. doi: 10.4319/lo.2008.53.3.0955

Hoikkala, L., Lahtinen, T., Perttila, M., and Lignell, R. (2012). Seasonal dynamics of dissolved organic matter on a coastal salinity gradient in the northern Baltic Sea. *Continental Shelf Res.* 45, 1–14. doi: 10.1016/j.csr.2012.04.008

Huang, X., Fu, X., Zhao, Z., and Yin, H. (2024). The telltale fluorescence fingerprints of sewer flows for interpreting the low influent concentration in wastewater treatment plant. *J. Environ. Manage.* 349, 349. doi: 10.1016/j.jenvman.2023.119517

Huang, R., Xie, L., Li, M., and Wang, L. (2021). Observational analysis on 3D distribution and seasonal variation of thermohaline characteristics in the Zhanjiang Bay. *Haiyang Xuebao* 43, 46–60. doi: 10.12284/hyxb2021156

Huguet, A., Vacher, L., Relexans, S., Saubusse, S., Froidefond, J. M., and Parlanti, E. (2009). Properties of fluorescent dissolved organic matter in the Gironde Estuary. *Organic Geochemistry* 40, 706–719. doi: 10.1016/j.orggeochem.2009.03.002

Jiang, T., Skyllberg, U., Bjorn, E., Green, N. W., Tang, J., Wang, D., et al. (2017). Characteristics of dissolved organic matter (DOM) and relationship with dissolved mercury in Xiaoqing River-Laizhou Bay estuary, Bohai Sea, China. *Environ. pollut.* 223, 19–30. doi: 10.1016/j.envpol.2016.12.006

Jiao, N., Luo, T., Chen, Q., Zhao, Z., Xiao, X., Liu, J., et al. (2024). The microbial carbon pump and climate change. *Nat. Rev. Microbiol.* 22, 408–419. doi: 10.1038/s41579-024-01018-0

Jiao, N., Tang, K., Cai, H., and Mao, Y. (2011). Increasing the microbial carbon sink in the sea by reducing chemical fertilization on the land. *Nat. Rev. Microbiol.* 9, 75–75. doi: 10.1038/nrmicro2386-c2

Kawasaki, N., and Benner, R. (2006). Bacterial release of dissolved organic matter during cell growth and decline: Molecular origin and composition. *Limnology Oceanography* 51, 2170–2180. doi: 10.4319/lo.2006.51.5.2170

Klinkhammer, G. P., McManus, J., Colbert, D., and Rudnicki, M. D. (2000). Behavior of terrestrial dissolved organic matter at the continent-ocean boundary from high-resolution distributions. *Geochimica Cosmochimica Acta* 64, 2765–2774. doi: 10.1016/S0016-7037(99)00370-1

Kothawala, D. N., Murphy, K. R., Stedmon, C. A., Weyhenmeyer, G. A., and Tranvik, L. J. (2013). Inner filter correction of dissolved organic matter fluorescence. *Limnology Oceanography: Methods* 11, 616–630. doi: 10.4319/lom.2013.11.616

Lao, Q., Chen, F., Jin, G., Lu, X., Chen, C., Zhou, X., et al. (2023b). Characteristics and mechanisms of typhoon-induced decomposition of organic matter and its implication for climate change. *J. Geophysical Research-Biogeosciences* 128, 128. doi: 10.1029/2023JG007518

Lao, Q., Lu, X., Chen, F., Chen, C., Jin, G., and Zhu, Q. (2023a). A comparative study on source of water masses and nutrient supply in Zhanjiang Bay during the normal summer, rainstorm, and typhoon periods: Insights from dual water isotopes. *Sci. Total Environ.* 903, 166853. doi: 10.1016/j.scitotenv.2023.166853

Lao, Q., Wu, J., Chen, F., Zhou, X., Li, Z., Chen, C., et al. (2022). Increasing intrusion of high salinity water alters the mariculture activities in Zhanjiang Bay during the past two decades identified by dual water isotopes. *J. Environ. Manage.* 320, 115815. doi: 10.1016/j.jenvman.2022.115815

Lawaetz, A. J., and Stedmon, C. A. (2009). Fluorescence intensity calibration using the raman scatter peak of water. *Appl. Spectrosc.* 63, 936–940. doi: 10.1366/000370209788964548

Lehmann, J., and Kleber, M. (2015). The contentious nature of soil organic matter. *Nature* 528, 60–68. doi: 10.1038/nature16069

Letscher, R. T., Hansell, D. A., and Kadko, D. (2011). Rapid removal of terrigenous dissolved organic carbon over the Eurasian shelves of the Arctic Ocean. *Mar. Chem.* 123, 78–87. doi: 10.1016/j.marchem.2010.10.002

Li, P., Chen, L., Zhang, W., and Huang, Q. (2015). Spatiotemporal distribution, sources, and photobleaching imprint of dissolved organic matter in the Yangtze Estuary and its adjacent sea using fluorescence and parallel factor analysis. *PloS One* 10, e0130852. doi: 10.1371/journal.pone.0130852

Li, M., Peng, C., Zhou, X., Yang, Y., Guo, Y., Shi, G., et al. (2019a). Modeling global riverine DOC flux dynamics from 1951 to 2015. *J. Adv. Modeling Earth Syst.* 11, 514–530. doi: 10.1029/2018MS001363

Li, Y., Song, G., Massicotte, P., Yang, F., Li, R., and Xie, H. (2019b). Distribution, seasonality, and fluxes of dissolved organic matter in the Pearl River (Zhujiang) estuary, China. *Biogeosciences* 16, 2751–2770. doi: 10.5194/bg-16-2751-2019

Liang, H., Zhang, J., Zhang, J., Zhang, P., Deng, X., Chen, J., et al. (2024). Unveiling the eutrophication crisis: 20 years of nutrient development in Zhanjiang Bay, China. *Front. Mar. Sci.* 11. doi: 10.3389/fmars.2024.1373716

Liu, S., Maavara, T., Brinkerhoff, C. B., and Raymond, P. A. (2022). Global controls on DOC reaction versus export in watersheds: A damkohler number analysis. *Global Biogeochemical Cycles* 36, e2021GB007278. doi: 10.1029/2021GB007278

Liu, M., Raymond, P. A., Lauerwald, R., Zhang, Q., Trapp-Müller, G., Davis, K. L., et al. (2024). Global riverine land-to-ocean carbon export constrained by observations and multi-model assessment. *Nat. Geosci.* 17, 896–904. doi: 10.1038/s41561-024-01524-z

Lønborg, C., Álvarez-Salgado, X. A., Davidson, K., and Miller, A. E. J. (2009). Production of bioavailable and refractory dissolved organic matter by coastal heterotrophic microbial populations. *Estuar. Coast. Shelf Sci.* 82, 682–688. doi: 10.1016/j.ecss.2009.02.026

Markager, S., Stedmon, C. A., and Søndergaard, M. (2011). Seasonal dynamics and conservative mixing of dissolved organic matter in the temperate eutrophic estuary Horsens Fjord. *Estuar. Coast. Shelf Sci.* 92, 376–388. doi: 10.1016/j.ecss.2011.01.014

Massicotte, P., Asmala, E., Stedmon, C., and Markager, S. (2017). Global distribution of dissolved organic matter along the aquatic continuum: Across rivers, lakes and oceans. *Sci. Total Environ.* 609, 180–191. doi: 10.1016/j.scitotenv.2017.07.076

McCallister, S. L., Bauer, J. E., Ducklow, H. W., and Canuel, E. A. (2006). Sources of estuarine dissolved and particulate organic matter: A multi-tracer approach. *Organic Geochemistry* 37, 454–468. doi: 10.1016/j.orggeochem.2005.12.005

McDonough, L. K., Andersen, M. S., Behnke, M. I., Rutlidge, H., Oudone, P., Meredith, K., et al. (2022). A new conceptual framework for the transformation of groundwater dissolved organic matter. *Nat. Commun.* 13, 2153. doi: 10.1038/s41467-022-29711-9

Medeiros, P. M., Seidel, M., Ward, N. D., Carpenter, E. J., Gomes, H. R., Niggemann, J., et al. (2015). Fate of the Amazon River dissolved organic matter in the tropical Atlantic Ocean. *Global Biogeochemical Cycles* 29, 677–690. doi: 10.1002/2015GB005115

Moran, M. A., Sheldon, W. M., and Zepp, R. G. (2000). Carbon loss and optical property changes during long-term photochemical and biological degradation of estuarine dissolved organic matter. *Limnology Oceanography* 45, 1254–1264. doi: 10.4319/lo.2000.45.6.1254

Murphy, K. R., Stedmon, C. A., Wenig, P., and Bro, R. (2014). OpenFluor- an online spectral library of auto-fluorescence by organic compounds in the environment. *Analytical Methods* 6, 658–661. doi: 10.1039/C3AY41935E

Osterholz, H., Kirchman, D. L., Niggemann, J., and Dittmar, T. (2016). Environmental drivers of dissolved organic matter molecular composition in the Delaware Estuary. *Front. Earth Sci.* 4. doi: 10.3389/feart.2016.00095

Raymond, P. A., and Spencer, R. G. M (2015). "Chapter 11 - Riverine DOM," in *Biogeochemistry of Marine Dissolved Organic Matter*, *2nd ed*. Eds. D. A. Hansell and C. A. Carlson (Academic Press, Boston), 509–533.

Rochelle-Newall, E. J., and Fisher, T. R. (2002). Production of chromophoric dissolved organic matter fluorescence in marine and estuarine environments: an investigation into the role of phytoplankton. *Mar. Chem.* 77, 7–21. doi: 10.1016/S0304-4203(01)00072-X

Romera-Castillo, C., Sarmento, H., Alvarez-Salgado, X. A., Gasol, J. M., and Marrase, C. (2010). Production of chromophoric dissolved organic matter by marine phytoplankton. *Limnology Oceanography* 55, 446–454. doi: 10.4319/lo.2010.55.1.0446

Safieddine, S. A., and Heald, C. L. (2017). A global assessment of dissolved organic carbon in precipitation. *Geophysical Res. Lett.* 44, 11,672–611,681. doi: 10.1002/2017GL075270

Søndergaard, M., Borch, N. H., and Riemann, B. (2000). Dynamics of biodegradable DOC produced by freshwater plankton communities. *Aquat. Microbial Ecol.* 23, 73–83. doi: 10.3354/ame023073

Spencer, R. G. M., Aiken, G. R., Dornblaser, M. M., Butler, K. D., Holmes, R. M., Fiske, G., et al. (2013). Chromophoric dissolved organic matter export from U.S. rivers. *Geophysical Res. Lett.* 40, 1575–1579. doi: 10.1002/grl.50357

Spencer, R. M., and Raymond, P. A. (2024). "Chapter 14 - Riverine DOM," in *Biogeochemistry of Marine Dissolved Organic Matter*, *3rd ed.* (Amsterdam, Netherlands: Academic Press), 657–691.

Stedmon, C. A., and Markager, S. (2005). Tracing the production and degradation of autochthonous fractions of dissolved organic matter by fluorescence analysis. *Limnology Oceanography* 50, 1415–1426. doi: 10.4319/lo.2005.50.5.1415

Stedmon, C. A., Markager, S., and Bro, R. (2003). Tracing dissolved organic matter in aquatic environments using a new approach to fluorescence spectroscopy. *Mar. Chem.* 82, 239–254. doi: 10.1016/S0304-4203(03)00072-0

Stedmon, C. A., Thomas, D. N., Papadimitriou, S., Granskog, M. A., and Dieckmann, G. S. (2011). Using fluorescence to characterize dissolved organic matter in Antarctic sea ice brines. *J. Geophysical Research-Biogeosciences* 116, G03027. doi: 10.1029/2011JG001716

Tromboni, F., Hotchkiss, E. R., Schechner, A. E., Dodds, W. K., Poulson, S. R., and Chandra, S. (2022). High rates of daytime river metabolism are an underestimated component of carbon cycling. *Commun. Earth Environ.* 3, 270. doi: 10.1038/s43247-022-00607-2

Tzortziou, M., Zeri, C., Dimitriou, E., Ding, Y., Jaffe, R., Anagnostou, E., et al. (2015). Colored dissolved organic matter dynamics and anthropogenic influences in a major transboundary river and its coastal wetland. *Limnology Oceanography* 60, 1222–1240. doi: 10.1002/lno.10092

Vidal, L. O., Lambert, T., Cotovicz, L. C. Jr., Bernardes, M. C., Sobrinho, R., Thompson, F., et al. (2023). Seasonal and diel modulation of DOM in a mangrove-dominated estuary. *Sci. Total Environ.* 857, 857. doi: 10.1016/j.scitotenv.2022.159045

Vystavna, Y., Chavanne, L., Harjung, A., Soto, D. X., Watson, A., Miller, J., et al. (2024). Predicting river flow dynamics using stable isotopes for better adaptation to climate and land-use changes. *Nat. Water* 2, 741–748. doi: 10.1038/s44221-024-00280-z

Wang, C., Hu, X., Liu, Y., and Jin, G. (2022). Sources, spectral characteristics, and fluxes of dissolved organic matter in coastal groundwater and river water in western Guangdong, China. *Front. Environ. Sci.* 10. doi: 10.3389/fenvs.2022.995190

Weishaar, J. L., Aiken, G. R., Bergamaschi, B. A., Fram, M. S., Fujii, R., and Mopper, K. (2003). Evaluation of specific ultraviolet absorbance as an indicator of the chemical composition and reactivity of dissolved organic carbon. *Environ. Sci. Technol.* 37, 4702–4708. doi: 10.1021/es030360x

Welschmeyer, N. A. (1994). Fluorometric analysis of chlorophyll a in the presence of chlorophyll b and pheopigments. *Limnology Oceanography* 39, 1985–1992. doi: 10.4319/lo.1994.39.8.1985

Wen, Z., Shang, Y., Lyu, L., Liu, G., Hou, J., He, C., et al. (2021). Sources and composition of riverine dissolved organic matter to marginal seas from mainland China. *J. Hydrology* 603, 127152. doi: 10.1016/j.jhydrol.2021.127152

Wu, Q., Ke, L., Wang, J., Pavelsky, T. M., Allen, G. H., Sheng, Y., et al. (2023). Satellites reveal hotspots of global river extent change. *Nat. Commun.* 14, 1587. doi: 10.1038/s41467-023-37061-3

Xia, B., and Zhang, L. (2011). Carbon distribution and fluxes of 16 rivers discharging into the Bohai Sea in summer. *Acta Oceanologica Sin.* 30, 43–54. doi: 10.1007/s13131-011-0118-3

Xiao, X., Powers, L. C., Liu, J., Gonsior, M., Zhang, R., Zhang, L., et al. (2022). Biodegradation of Terrigenous Organic Matter in a Stratified Large-Volume Water Column: Implications of the removal of terrigenous organic matter in the coastal ocean. *Environ. Sci. Technol.* 56, 5234–5246. doi: 10.1021/acs.est.1c08317

Ya, C., Anderson, W., and Jaffe, R. (2015). Assessing dissolved organic matter dynamics and source strengths in a subtropical estuary: Application of stable carbon isotopes and optical properties. *Continental Shelf Res.* 92, 98–107. doi: 10.1016/j.csr.2014.10.005

Yamashita, Y., Fichot, C. G., Shen, Y., Jaffe, R., and Benner, R. (2015). Linkages among fluorescent dissolved organic matter, dissolved amino acids and lignin-derived phenols in a river-influenced ocean margin. *Front. Mar. Sci.* 2, G00F10. doi: 10.3389/fmars.2015.00092

Yamashita, Y., Jaffe, R., Maie, N., and Tanoue, E. (2008). Assessing the dynamics of dissolved organic matter (DOM) in coastal environments by excitation emission matrix fluorescence and parallel factor analysis (EEM-PARAFAC). *Limnology Oceanography* 53, 1900–1908. doi: 10.4319/lo.2008.53.5.1900

Yamashita, Y., Maie, N., Briceno, H., and Jaffe, R. (2010). Optical characterization of dissolved organic matter in tropical rivers of the Guayana Shield, Venezuela. *J. Geophysical Research-Biogeosciences* 115. doi: 10.1029/2009JG000987

Yamashita, Y., and Tanoue, E. (2003). Chemical characterization of protein-like fluorophores in DOM in relation to aromatic amino acids. *Mar. Chem.* 82, 255–271. doi: 10.1016/S0304-4203(03)00073-2

Yang, L., Cheng, Q., Zhuang, W.-E., Wang, H., and Chen, W. (2019). Seasonal changes in the chemical composition and reactivity of dissolved organic matter at the land-ocean interface of a subtropical river. *Environ. Sci. pollut. Res.* 26, 24595–24608. doi: 10.1007/s11356-019-05700-2

Yang, L., Hong, H., Chen, C.-T. A., Guo, W., and Huang, T.-H. (2013). Chromophoric dissolved organic matter in the estuaries of populated and mountainous Taiwan. *Mar. Chem.* 157, 12–23. doi: 10.1016/j.marchem.2013.07.002

Zhang, J., Zhang, Y., Zhang, P., Li, Y., Li, J., Luo, X., et al. (2021). Seasonal phosphorus variation in coastal water affected by the land-based sources input in the eutrophic Zhanjiang Bay, China. *Estuarine Coast. Shelf Sci.* 252, 107277. doi: 10.1016/j.ecss.2021.107277

Zhao, C., Zhou, Y., Pang, Y., Zhang, Y., Huang, W., Wang, Y., et al. (2021). The optical and molecular signatures of DOM under the eutrophication status in a shallow, semi-enclosed coastal bay in southeast China. *Sci. China-Earth Sci.* 64, 1090–1104. doi: 10.1007/s11430-020-9728-4

Zhong, J., Pan, P., Xiao, S., and Ouyang, X. (2022). Influence of eucalyptus plantation on soil organic carbon and its fractions in severely degraded soil in Leizhou Peninsula, China. *Forests* 13, 1606. doi: 10.3390/f13101606

Zhuang, W.-E., Chen, W., Cheng, Q., and Yang, L. (2021). Assessing the priming effect of dissolved organic matter from typical sources using fluorescence EEMs-PARAFAC. *Chemosphere* 264, 128600. doi: 10.1016/j.chemosphere.2020.128600

Zsolnay, A., Baigar, E., Jimenez, M., Steinweg, B., and Saccomandi, F. (1999). Differentiating with fluorescence spectroscopy the sources of dissolved organic matter in soils subjected to drying. *Chemosphere* 38, 45–50. doi: 10.1016/S0045-6535(98)00166-0